How SLKP peptoid inhibits $A\beta_{42}$ self-aggregation in Alzheimer's disease: A molecular dynamics investigation

A

Dissertation submitted

in partial fulfilment of the requirements for the degree of

Master of Science

In

Chemistry

by

Sagrika Shukla

(Reg. No: 301702027)

Under the Supervision of

Dr. Bhupesh Goyal

SCHOOL OF CHEMISTRY AND BIOCHEMISTRY

THAPAR INSTITUTE OF ENGINEERING AND TECHNOLOGY, PATIALA-147004

July 2019

CERTIFICATE

This is to certify that the thesis entitled "**How SLKP peptoid inhibits Aβ$_{42}$ self-aggregation in Alzheimer's disease: A molecular dynamics investigation**" being submitted by **Ms. Sagrika Shukla** in partial fulfilment of requirements for the award of degree of **Master of Science** in **Chemistry** and being submitted to the School of Chemistry and Biochemistry, Thapar Institute of Engineering and Technology, Patiala is a bonafide work carried out by her under my supervision. The work has reached the standard necessary for submission and the content of this report has not previously formed the basis for award of any degree, or other similar title or recognition.

Bhupesh Goyal

Dr. Bhupesh Goyal
Assistant Professor
School of Chemistry & Biochemistry
Thapar Institute of Engineering & Technology, Patiala-147004

Countersigned by

Dr. Amjad Ali
Professor & Head
School of Chemistry & Biochemistry
Thapar Institute of Engineering & Technology, Patiala-147004

DECLARATION

I hereby declare that the thesis being presented, entitled "**How SLKP peptoid inhibits Aβ$_{42}$ self-aggregation in Alzheimer's disease: A molecular dynamics investigation**" is a legitimate record of my work for the fulfilment of requirements of award of degree of Master of Science in Chemistry at Thapar Institute of Engineering and Technology, Patiala under the supervision of Dr. Bhupesh Goyal, Assistant Professor, School of Chemistry and Biochemistry, Thapar Institute of Engineering and Technology, Patiala during January 2019 to July 2019. This report has not previously formed the basis for award of any degree, or other similar title or recognition.

Sagrika

Date: 14.08.2019

Sagrika Shukla

It is certified that the above statement made by the student is correct to the best of my knowledge and belief.

Bhupesh Goyal

Dr. Bhupesh Goyal
Assistant Professor
School of Chemistry & Biochemistry
T.I.E.T, Patiala-147004

Dr. Amjad Ali
Professor & Head
School of Chemistry & Biochemistry
T.I.E.T, Patiala-147004

ACKNOWLEDGMENT

I would like to use this opportunity to express my deepest appreciation to all the individuals for sharing their pearls of wisdom throughout the course of this project.

First of all I would like to thank **Dr. Amjad Ali** for providing me an opportunity to get myself exposed to the field of research through this dissertation. I am highly grateful to my Supervisor **Dr. Bhupesh Goyal** for his valuable time, guidance and persisting support during the whole project.

I would like to acknowledge Miss Rajneet Kaur Saini, Mr. Simranjeet Singh, Mrs. Rajdeep Kaur and Mrs. Apneet Kaur for their technical guidance, effectual efforts and enduring support.

I am thankful to **Thapar Institute of Engineering and Technology and School of Chemistry & Biochemistry** for providing me the well-equipped infrastructure.

Further I am highly obliged to my family and friends for consistent encouragement and succor.

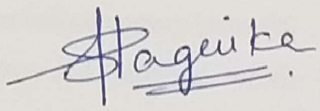

Sagrika Shukla

Abstract

Amyloid-β (Aβ) aggregation, a key pathological hallmark of Alzheimer's disease (AD) leads to formation of insoluble oligomers and fibrils which gets deposited in interstitial spaces of brain resulting in loss of intellectual functioning of brain. From last decade, peptidomimetically derived peptoids have shown proficient pharmacokinetic properties against AD. Recently, SLKP peptoid, displaying significant neuro-protection and neuro-regeneration against Aβ toxicity and its ability to cross blood brain barrier was reported. The *in vivo* and *in vitro* results shows that SLKP inhibit the self-aggregation of $A\beta_{42}$. However the exact mechanism of inhibition of amyloid aggregation by SLKP is not reported. In this regards, in the present study the molecular mechanism by which SLKP inhibits $A\beta_{42}$ monomer aggregation has been elucidated using molecular docking and molecular dynamics (MD) simulations. Molecular docking analysis highlights that SLKP shows interaction with the N-terminal region of $A\beta_{42}$ monomer. To find out the big picture, explicit type MD of $A\beta_{42}$ monomer alone and in presence of SLKP was performed. MD analysis highlighted that SLKP efficiently obstructed conformational transition and stabilizes the native helical structure of $A\beta_{42}$ monomer by interacting with N-terminal region, and C-terminal region. The clustering analysis shows the conformations, in which SLKP interact with the N and C-terminal region of $A\beta_{42}$ monomer, blocking the self-aggregation of $A\beta_{42}$ monomer form both terminal. Secondary structure analysis shows that SLKP remarkably intensifies the helical content from 5% to 37% in Aβ monomer and prevents the formation of β-sheet structure at C-terminal, which demonstrated the conservation of native structure of $A\beta_{42}$ monomer in presence of SLKP. MM-PBSA analysis highlighted that Asp7, Ser8, Gly9, His13, Val18 and Ala21 were found to be the key residues of $A\beta_{42}$ monomer that participated in binding with SLKP. The insights into the underlying inhibitory mechanism of SLKP against Aβ aggregation will be lucrative for peptoid based therapeutics against AD in future.

Contents

List of figures

List of tables

List of abbreviations & symbols

Abbreviation/Symbol	Full Name/ Meaning
$A\beta_{42}$	Amyloid Beta
AD	Alzheimer's Disease
APP	Amyloid Precursor Protein
BACE I	β-site Amyloid Precursor Protein Cleaving Enzyme 1
BBB	Blood Brain Barrier
DSSP	Dictionary of Secondary Structures of Proteins
FEL	Free Energy Landscape
FTIR	Fourier Transform Infrared Spectroscopy
GADPH	Glyceraldehyde 3-phosphate dehydrogenase
GROMACS	GROningen Machine for Chemical Simulations
HBA	Hydrogen Bond Acceptor
HBD	Hydrogen Bond Donor
KV	Potassium Channel
LMMC	Local move Monte Carlo
MD	Molecular Dynamics
MM-PBSA	Molecular Mechanics / Poisson–Boltzmann Solvent-Accessible Surface Area
NFT	Neurofibrillary Tangles
NMR	Nuclear Magnetic Resonance
PDB	Protein Data Bank
PSEN 1	Presenilin-1

PSEN 2	Presenilin-2
R_g	Radius of Gyration
RMSD	Root Mean Square Deviation
RMSF	Root Mean Square Fluctuation
SLKP	Ser-Leu-Lys-Pro
TEM	Transmission Electron Microscopy
ThT	Thioflavin T
TP	Tyrosine Phosphate

1. Introduction

The loss of structure or function of nerve cell or nervous system with time causes the occurrence of neurodegenerative disease.[1] One of the fatal neurodegenerative disease is Alzheimer disease which is affecting 50 million people globally, and according to estimations, it will hit 82 million by 2030.[2] Dementia with age and loss of intellectual functions are major symptoms shown by AD. The exact etiology of AD is unclear but it is considered to be a result of protein misfolding found in form of "senile plaques" in the brain.[3] Protein misfolding leads to formation of insoluble aggregates which are found to be the candid reason of most diseases. According to the amyloid hypothesis, Amyloid Precursor Protein (APP), which is a trans-membrane protein, gets cleaved by β-secretase followed by γ-secretase which produces short insoluble peptide fragments (β Amyloid). The cleaved products constitute $A\beta_{40}$ and $A\beta_{42}$ in ratio 9:1. Normal human brain has 80% $A\beta_{40}$, but AD brain has excess of $A\beta_{42}$ which is hydrophobic due to presence of two additional C-terminal residue.

The main cause of amyloid aggregation is transformation of α-helical conformation into β-sheet structure and its assembly led into formation of fibrillar structure,[4] which virulently affects key intracellular causeway concluding to nervous breakdown. The aggregates of oligomeric and fibrillar structures of Aβ species forges it to toxicity and this mechanism is acknowledged as the amyloid cascade hypothesis. The crucial nucleation step involves the concentration of monomeric structure of Aβ that affects the genesis of fibrillar aggregates through which oligomeric species are produced. The fibrillar species prompts the generation of oligomeric structures, after the formation of fibrillar structure through first crucial step, which is known as secondary nucleation. The toxicity of the oligomeric structures are way higher than the presence of mature fibrillar structures.[5]

Literature has reported different methods which are being appraised to inhibit the development of fibrils and toxic oligomers. There are so many small molecules[678] which have been successful amyloid aggregation inhibitors but none has been therapeutically successful. From last decade, in literature various studies are reported in which natural and modified peptides are identified as inhibitors of amyloid aggregation. Barale et al., showed that the peptide containing Arg amino acid can destabilize the preformed Aβ protofibril aggregation.[9] Viet et al., showed natural peptide LPFFD disaggregates the oligomeric structure of amyloid peptide Aβ.[10] Jagota et al., showed that

the short D-peptides PGKLVYA, KKLVFFARRRA, and KKLVFFA have shown promising results at inhibiting the aggregation of Aβ monomer.[11] Moreover Ashur-Fabian et al., discovered that NAPVSIPQ octapeptide decreases the aggregation of Aβ by 40%.[12] Granic et al., revealed that LPYFD can reserve intellect by retrogressing $A\beta_{42}$ oligomer instigated learning deficiency.[13] In spite of the ability of peptides to inhibit amyloid aggregation and give information about the amyloid aggregates themselves[14] they are not therapeutically accomplished because of their poor BBB (Blood brain barrier) permeability and lower bioavailability.[15]

So a new approach has been followed in this direction where poly-N-substituted glycines (peptoids) have been developed which belong to a category of small chain of peptides that are different from peptides, as these have side chain attached to nitrogen atom of amide group. Due to this structural variation peptoids were found to be resistant to protease degradation and hence have desirable bioavailability.[16,17] Pradhan et al., has reported SLKP peptoid which has shown eminent results *in vitro* and *in vivo* assays like it significantly inhibited Aβ fibrillization, shown noteworthy protection against toxicity caused by amyloid formation, promoted notable neuron growth, maintained healthy morphology of rat cell neurons.[4] In this report we have adopted the molecular modelling approach to analyze the mechanistic details through which the SLKP has inhibited the self-aggregation of amyloid $A\beta_{42}$ monomer. Docking results showed that SLKP showed strong interaction with Aβ peptide (-4.4 kcal/mol) through hydrogen bonding and hydrophobic interactions. Molecular dynamics (MD) simulations revealed that SLKP successfully inhibits amyloid aggregation and hence stabilizes the helical conformation of $A\beta_{42}$ monomer.

2. Literature Review

---

1. Pradhan, K. et al. ACS Chem. Neurosci. **2019**, *10*, 1355-1368.[5]

In this paper, the authors have reported Ser-Leu-Lys-Pro (SLKP) peptide which is derived from a dodeca-neuropeptide found in brain of frog. Further they have synthesized SLKP peptoid by adopting peptidomimetic approach. It has shown remarkable potency in neuroprotection than its peptide analogue. It is the shortest peptoid reported so far which remarkably inhibits Aβ oligomerization and fibrillization, shows notable neuroprotection against Aβ mediated toxicity and efficiently crosses Blood Brain Barrier (BBB). SLKP peptoid also binds to tubulin and aids tubulin polymerization along with lowered energy status of microtubule networks. It is stable in serum and fosters neurite outgrowth.

2. Mehrazma, B. et al. J. Phys. Chem. A **2019**, *22*, 4658-4670.[18]

In this paper, the authors have probed about the dimer structure of amyloid-beta i.e. the smallest toxic Aβ oligomers by performing a total of 9.5μs molecular dynamics simulation. The paper has reported different feasible structures of Aβ dimers and their relative binding affinity. Further seven poses have been chosen from docking studies as beginning structures for MD and then the most stable was subjected to another long-time MD simulation. The results showed that the most stable structure has maximum number of intermolecular β sheets i.e. two R-SHR interactions and one SHR-N terminal β sheet interaction. Another stable structure possess extended R-R' sheet along with small SHR-N-Terminal' and R-C Terminal' interaction. Hence this study demonstrates the importance of hydrophobic and terminal regions in accumulation and lowered energy of dimer structure. So N-terminal region should be one of the target site for the eligible amyloid inhibitor.

3. Barale, S. S. et al. ACS Omega **2019**, *4*, 892-903.[9]

In this paper, the authors have highlighted the mechanism by which RR-AFC destabilizes and obstructs the aggregation of Aβ protofibril. Hydrogen bonding was found to be the key interaction through which RR-AFC binds to Aβ protofibril. It has also been observed from MD simulations that RR-AFC binds to the edge of chain- A and Aβ protofibril has been destabilized by hydrophobic

core. The firmly packed protofibrils of β–sheet are opened due to loss of hydrophobic contacts. The major factor which destabilizes Aβ protofibril was the hydration of salt bridge between Lys28 and RR–AFC. It has been observed from free energy calculations that van der Waals interactions are most dominant. The results of above article reveals that in designing new inhibitors against Aβ aggregation, the structural information of inhibitor plays a notable role.

4. Young, S. C. et al. Molecules **2018**, *23*, 296, DOI: 10.3390/molecules23020296.[19]

In this review, the author has mentioned that peptoids have better pharmacokinetic properties than peptides and significant steps that have been made in the area of salubrious peptoids as shown in Fig. 1. Various peptoids have been mentioned which have anti amyloidogenic properties and many metal-chelating peptoids are bestowed which can be proven to be effective against AD. He has mentioned many peptoid-based Aβ1–40 and Aβ1–42 accretion obstructers out of which some were selective or BBB permeable. In the light of the relationship between Aβ-accretion, AD pathology, and metal dysregulation, these atoms establish a blessed future bearing. Peptoids that have been talked about are not only exclusive to biological functions pertinent to AD, they can possibly settle a significant number of the pharmacokinetic issues encompassing conventional

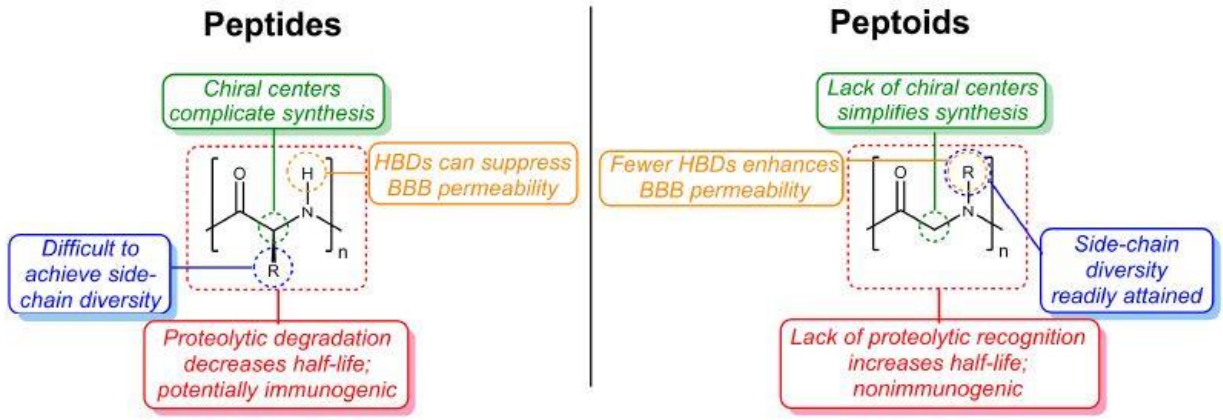

Figure 1: Advantages of peptoids over peptides.[19]

peptide-based therapeutics. As enormous structural variety can be accomplished with peptoids, this class of molecules can be promptly adjusted to consolidate various functionalities. From this review it is clear that peptoids have efficiency of becoming eminent drugs against amyloid aggregation and

other anti-bacterial, anti-cancer activity etc. As they have multiple beneficial actions, working on them will give positive outcomes.

5. Baig, M. H. et al. Front. Aging Neurosci. **2018**, DOI: 10.3389/fnagi.2018.00021.[20]

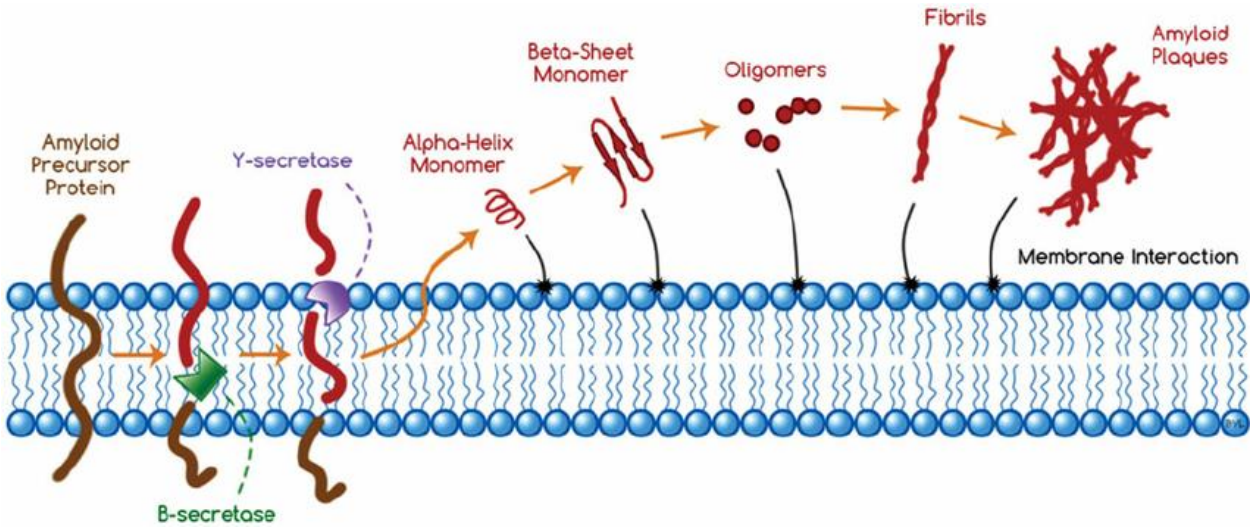

Figure 2: Process of Aβ aggregation.[20]

In this mini review, the authors have briefly discussed about the use of peptide-based compounds for pre-diagnosis and treatment of AD. Along with it they have mentioned about the peptide based inhibitors and their application against AD targets like amyloid beta, (BACE1), (GAPDH), (TP) and KV1.3. Here the authors have very proficiently mentioned about the schematic process of Aβ-fibril formation (Fig. 2) and use of peptides in inhibiting aggregation at different stages of amyloid aggregation. Further they have mentioned about various peptides that have been reported in literature from past decade which have shown effective results in prevention of aggregation (Table 1).

S. No.	Peptides	Description	References
1.	RGKLVFFGR (OR1) RGKLVFFGR-NH2 (OR2)	Based on the Aβ (16-20) sequence	Austen et al. (2008)
2.	Fc-KLVFF	Based on the Aβ (16-20) sequence and conjugated with ferrocenoyl (Fc)	Wei et al. (2011)
3.	KLVF-ΔA-I-ΔAKF-ΔA-ΔA-ΔA-F	Based on the Aβ (16-20) sequence and ΔAla	Wei et al. (2011)
4.	KLVFFA,KKLVFFA,KFVFFA,KIVFFA and KVVFFA	Based on the Aβ (16-20) sequence and replacement of L-with D-amino acids	Chalifour et al. (2003)
5.	PGKLVYA, KKLVFFRRRRA and KKLVFFA	d-peptides of Aβ (16-20)	Jagota and Rajadas (2013)
6.	RYYAAFFARR	Based on the Aβ (11-23)	Liu et al. (2014)

Table 1: Peptide-based inhibitors reported to be effective against Alzheimer's disease (AD). [20]

6. Chiti, F. et al. Annu. Rev. Biochem. **2017**, *86,* 27-68.[21]

In this review, the authors have looked into various physiochemical, biochemical, genetic and biological expositions of amyloid aggregation phenomenon to identify its common and generic features and their consequences with specific citation to the progress that have been made over a decade ago in this field. They have listed various disorders as well as the proteins that are associated which get deposited as amyloid or other type of clusters in human tissues. They have also mentioned about the proteins that play particular functional role in humans by exploiting amyloid motifs. Various genetic factors that provide a deep understanding of the way in which disease onset occurs have been encapsulated here. Various advances that have been made in understanding the structures of amyloid fibrils, their amyloidic oligomeric precursors and the way in which they are forged and escalated leading to cellular dysfunction have been discussed. They have shown corroborative evidences which reveal that under certain circumstances, a complex proteostasis network fails in fighting protein aggregation which gives rise to disease. Finally they have mentioned about the advancement in development of therapeutic strategies that are being followed from last decades i.e. from small organic molecules to naturally occurring peptide-based inhibitors.

7. Soto, C. et al. Nat. Rev. Neurosci. **2003**, *4,* 49-60.[22]

In this article, the author has put emphasis on molecular way in which protein misfolding occurs, its aggregation and participation in neurodegeneration. Three models of the molecular pathway of neurodegeneration related to protein misfolding and aggregation have been discussed extensively. Although the starting and the end of the pathway are similar in all hypothesis but the phenomenon that lead to neuronal death are different. It has been referenced that the absence of movement of local proteins is the key advance in Loss-of-work Hypothesis, in Gain-of- lethal action model, the critical advance is the procedure of neurotoxicity of the misfolded or accumulated protein and in Inflammation Hypothesis, enactment of astroglial cells prompts neuronal demise in a roundabout way (Fig. 3). In AD, neurodegeneration follows loss-of-function hypothesis. At the end various restorative techniques to capture protein misfolding and accumulation have been taken into consideration.

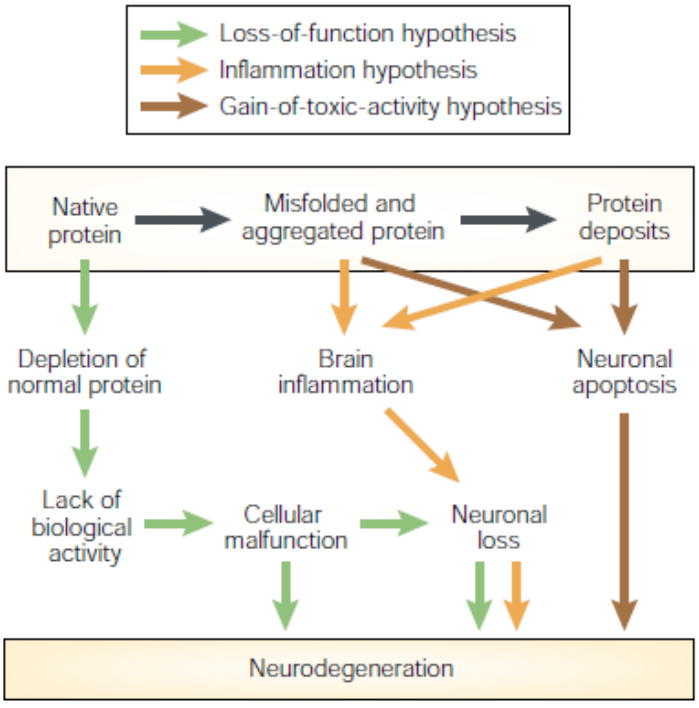

Figure 3: Models of Mechanism of neurodegeneration associated with protein misfolding and aggregation.[22]

8. Lane, C. A. et al. Eur. J. Neurol. **2018**, *25*, 59-70.[3]

In this review article, the spread, control, pathological factors, role of genetics and pathogenesis of Alzheimer's disease has been discussed in detail.

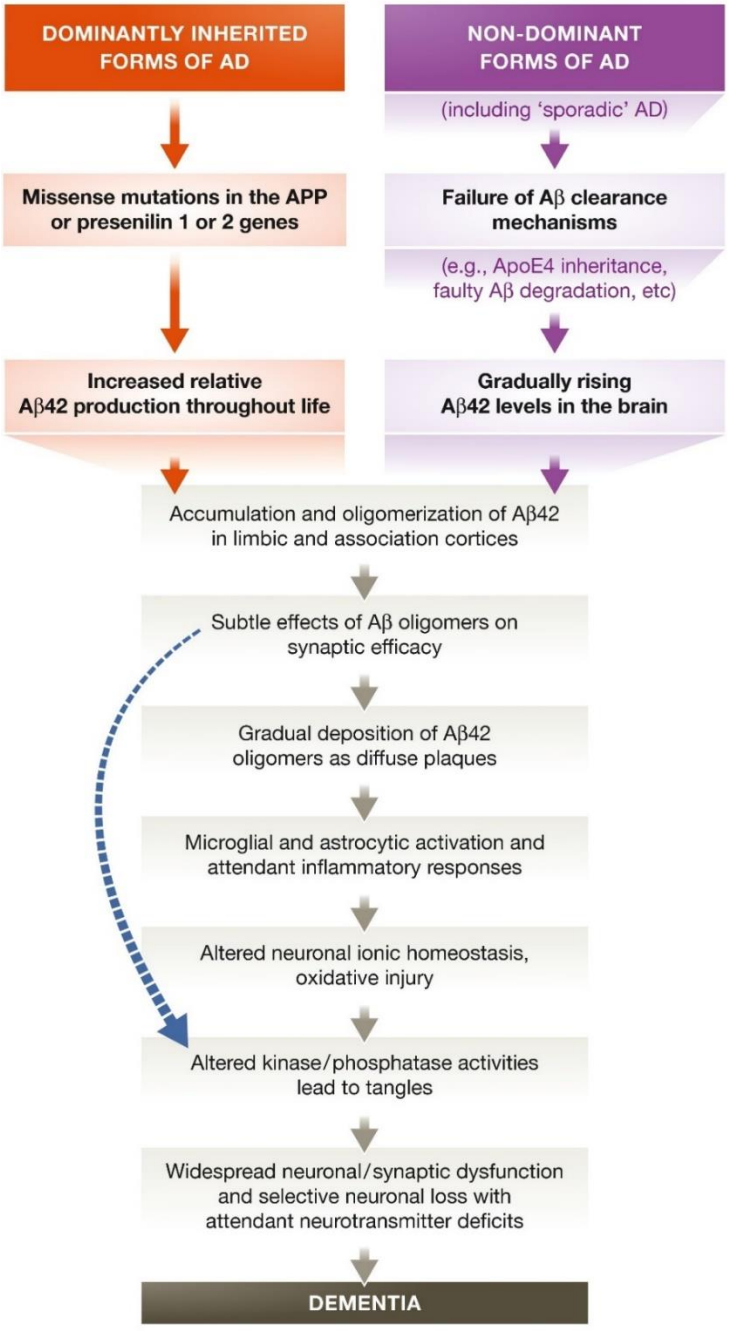

Figure 4: Major pathogenic events leading to Alzheimer's disease.[23]

It has been reported that the most common symptom of AD is dementia which leads to inability in thinking, remembering and behaving normally. The ratio of causing factors varies as 70: 30 where

70 % is attributed to genetic factors (mutation in APP, PSEN1, PSEN2 gene) and 30% is attributed to environmental factors also known as sporadic AD (Fig. 4). The two main pathological features neurofibrillary tangles and amyloid plaques. Along with these neuropil threads, dystrophic neuritis, astrogliosis and microglial activation are also observed. The formation of amyloid plaques is explained by amyloid cascade theory and NFTs are clumps of tau proteins which change their shape after getting phosphorylated and aggregates. Further the diagnostic features and treatment measures that have been done so far have been discussed.

9. Meng, X. Y. et al. Curr. Comput. Aided Drug Des. **2011**, *7,* 146-157.[24]

In this review, the authors have mentioned about the prevailing molecular docking ways, their growth and role in drug discovery. The differences in the algorithms used and performances for different docking tools have been given. Flexible ligand and rigid receptor docking where ligand can bind flexibly to rigid receptor has been annealed in Autodock 3.0 version. Further Soft docking has been mentioned which follows flexible ligand and flexible receptor docking approach. Local move Monte Carlo (LMMC) loop prediction approach has been attributed as most appropriate approach for flexible receptor docking. This approach has been considered computationally lucrative as it provides the ability of adjustment of extent of flexibility and user has been provided with the facility to control the side chain or full movement of the loop. It has shown that computational tools have proven to be powerful approach to screen hit big databases and design new molecules.

10. Durrant, J. D. et al. BMC Biol. **2011**, *9,* 71, DOI: 10.1186/1741-7007-9-71.[25]

In this review, the authors have discussed the role of atomistic simulations of macromolecules and small ligands in drug discovery. They have discussed briefly the pathway which is followed in molecular dynamics simulation. It has been mentioned that first the computational model of ligand receptor is generated, then molecular forces acting on each atom is calculated and accordingly each atom is moved following Newton's Laws of motion. This advanced simulation method is repeated many times. Further the limitations of MD are discussed. It has been mentioned that MD simulations are best tools for identifying allosteric and cryptic binding sites.

MD plays an important role in directly predicting ligand binding energies and enhancing virtual-screening methodologies. MD simulations fill the gap of shortcomings of experimental ways.

3. Research Gap

If we look into the literature so far on AD, there is still very little known about the definitive cause and suitable drug required for targeting AD. The most common type of symptoms includes memory loss and confused personality which eventually leads to the point where the victim gets completely out of touch with the surroundings. It is a leading cause of death worldwide from past few decades and is maintaining its increase rate exponentially. Till date there is no definitive drug which directly targets the causing agents *i.e.* the amyloid plaques and neurofibrillary tangles. Numerous studies from literature has shown that a great number of strategies have been appraised to inhibit the amyloid aggregation hence hampering the formation of toxic oligomers and fibrils. It is seen that generally two major strategies have been opted by researchers so far: First one is obstructing the amyloid formation by inhibitors and second one is based on using inhibitors to abolish the fibrils or oligomers that have been already formed. By using small organic molecules, nano-particles, peptide-based inhibitors and peptoids, the inhibition of amyloid fibrils and oligomers can be accomplished.

The inhibitory action of organic molecules is not prominent due to their small size as compared to the size of amyloid protein. Peptide-based inhibitors are comparatively better because of their more selectivity, effectiveness, low accumulation in tissues but they have low bio-availability and low BBB Permeability due to their big size, polarity, and huge number of HBDs and HBAs which makes them inadequate in spite of having so many favorable characters required for amyloid inhibition. The peptoids belong to a class of peptidomimetics that differ from peptides in having side chain attached to amide group instead of α-carbon. Due to this structural variation peptoids were found to be resistant to protease degradation and hence have desirable bioavailability *i.e.* they can efficiently cross BBB thereby having suitable pharmacokinetic properties for amyloid inhibition.

Herein we are dealing with SLKP peptoid which is the shortest peptoid to show neuroprotection and neurogeneration against Aβ toxicity. Experimental study has reported that many *in vitro* and *in vivo* assays have been performed on SKLP peptoid to study its ability to inhibit amyloid aggregation as well as obstruct pre-existing fibrils. FTIR study has revealed that SLKP peptoid did not show any β-sheet even after seven days of incubation, Dot Blot assay showed that SLKP can reduce the

fibril formation and oligomeric aggregation upto 78%, TEM study also revealed inhibiting action of SLKP on fibril formation. ThT assay showed that in presence of SLKP the fluorescence intensity of ThT was decreased which clearly indicates the inhibition of oligomeric aggregation in its presence. Moreover it can dissociate the pre-existing amyloid fibrillar structure. Isothermal Titration Calorimetry experiment revealed that the binding of SKLP peptoid with $A\beta_{42}$ monomer was exothermic in nature with binding stoichiometry of 1:1. BBB experiment showed that SLKP peptoid can cross BBB as SLKP mass was found in mass spectra. Although these results indicate the potency of SKLP peptoid as a proficient therapeutic agent, however the inhibitory mechanism by which SLKP peptoid obstructs oligomeric aggregation and fibril formation is still unknown.

Role of MD and molecular docking in drug discovery: Experimental studies alone are not adequate to clarify the inhibitory path followed by various inhibitors. The computational procedures give an elective methodology in deciding the protein–ligand interactions at an atomic level, which, generally, are hard to clarify utilizing exploratory strategies[26,27,28] MD and related techniques are near getting to be standard computational tools for drug discovery.[29] This permits an increasingly precise gauge of the thermodynamics and kinetics related with drug-target recognition and binding.

4. Objectives

- To elucidate the binding sites of $A\beta_{42}$ monomer which shows interaction with the SLKP peptoid using molecular docking.
- To find out the various possible interactions between $A\beta_{42}$ monomer and SLKP peptoid using computational techniques.
- To find out the overall inhibitory mechanism by which SLKP peptoid inhibit the self-aggregation of $A\beta_{42}$ monomeric structure using MD simulations.

5. Methodology

5.1 Modeling of SLKP peptoid

The structure of SLKP peptoid was drawn using ChemDraw version 15.0 (Fig. 5), and then the structure was optimized using Chem3D, version 15.0.

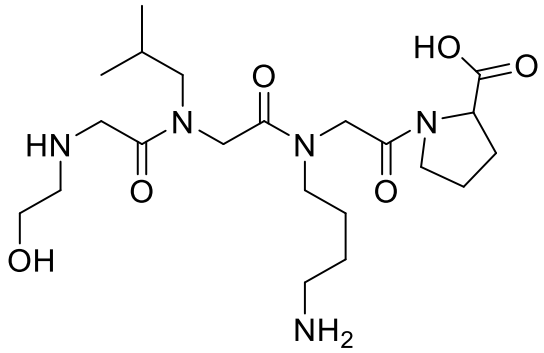

Figure 5: Chemical structure of SLKP peptoid.

5.2 Energy minimization of SLKP peptoid

The energy of SLKP peptoid was minimized using Chem3D, version 15.0, and Maestro_2019 1_Linux-x86_64_Academic to obtain optimized structure.

5.3 Molecular docking

The blind molecular docking was performed using Autodock Vina.[30] The dimension of the box was set to 114Å × 68Å × 126Å with grid Centre defined at x = -0.081, y = 0.018, z = 0.16. The output docked file was saved in PDBQT format and binding affinity was assessed.

5.4 Parameter generation of SLKP peptoid

The parameters of the SLKP peptoid were generated using ATB (Automated Topology Builder).[31]

5.5 *MD simulation*

The GROMACS 5.0.1[32] package was used to perform the MD simulations. The GROMOS96 54a7 force field[33] was used for simulations, which has been used in number of studies to elucidate the protein dynamics in explicit solvent. In our study, two systems were prepared, one is $A\beta_{42}$ monomer in water and the second is $A\beta_{42}$ monomer in presence of SLKP peptoid explicitly surrounded by water molecules. The two systems are named as $A\beta_{42}$ monomer and the next one is $A\beta_{42}$ monomer-SLKP complex. Both the systems were solvated by SPC216 water model and all the amino acids protonation state were assigned according to the pH 7.4. To neutralize the overall system number of counter ions were added and periodic boundary conditions were applied in all the three directions. Both the systems were energy minimized with the steepest decent integrator and all bonds was constrained using LINCS algorithm.[34] The short range electrostatic and van der Waals interactions were updated after 20 fs and the cut off value was kept 1.0 nm for MD simulations. The PME method[35] was used to calculate the long range electrostatic interactions. The equilibrium of the systems were followed after minimization step for both the systems.[36] For equilibration NVT conditions were used for 500 ps leading to next step of equilibration in which NPT environments were provided for 500 ps at 300K. The final MD simulations were performed for 200 ns each at constant pressure conditions with time step of 10 ps.

5.6 Data analysis

All the final MD simulation trajectories were investigated using in built tools of GROMACS, visual molecular dynamics (VMD), [37] and PyMOL softwares. [38] The clustering of obtained MD structures was performed using the Daura, et al., algorithm, in which 0.20 nm backbone[39] RMSD cut off was used. The different structural changes occurring in the systems were investigated by performing three GROMACS utilities such as gmx rms, gmx gyrate and gmx rmsf respectively. The changes in the secondary structure of proteins in both the systems were evaluated using DSSP by employing gmx do_dssp tool.[40] The overall summary of computational details and methods used are shown in Fig. 6.

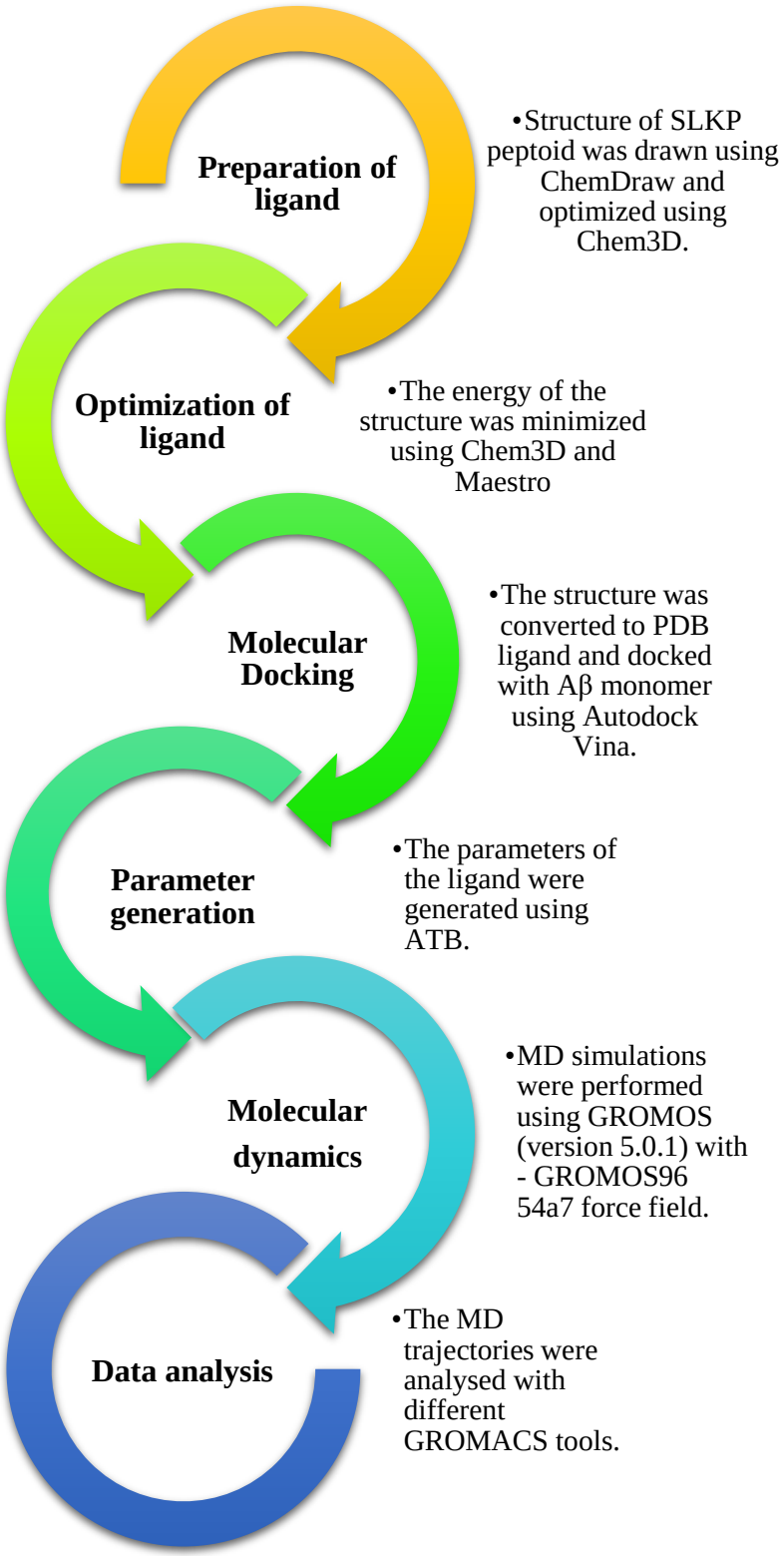

Figure 6: Summary of computational details.

6. Results and discussion

6.1 Prediction of binding region and key interactions with molecular docking

To explore the favored binding region and important interactions, blind molecular docking was performed using Autodock–Vina software, whereas AutoDock Tools was used to prepare PDBQT files for receptor and peptoid. Molecular Docking results showed that SLKP peptoid (Fig. 7a) binds to the N-terminal of $A\beta_{42}$ monomer (PDB ID 1IYT) (Fig. 7b) with negative binding energy (-4.4 kcal/mol) showing hydrogen bonding and hydrophobic interactions.

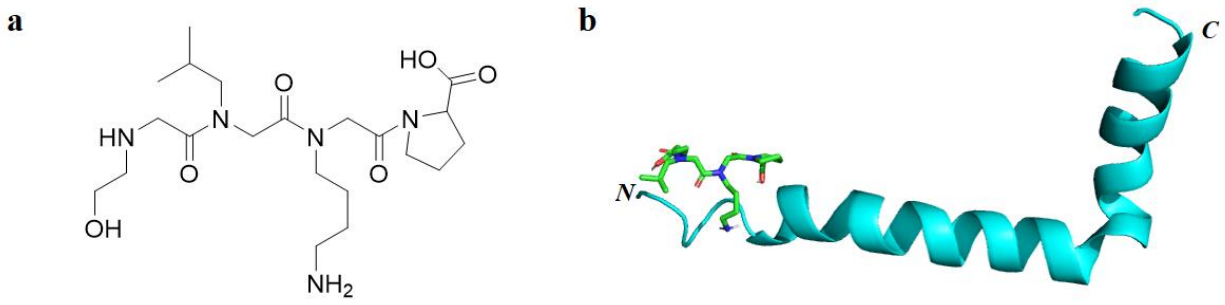

Figure 7: Chemical Structure of SLKP peptoid is shown in (panel a) and binding of SLKP peptoid with $A\beta_{42}$ monomer is shown in (panel b) respectively.

Three residues (Ser1, Lys3 and Pro4) of SLKP peptoid interacted with N-terminal residues Ala2, Glu3 and His6 of $A\beta_{42}$ monomer by forming four hydrogen bonds. The main chain oxygen atom of Ala2 was involved in hydrogen bond formation with main chain nitrogen of Ser1 of peptoid (0.30 nm). The main chain oxygen atom of Glu3 was involved in hydrogen bond with side chain nitrogen of Lys3 of peptoid (0.21 nm). His6 was involved in two hydrogen bond formation, one between side chain nitrogen atom and main chain oxygen atom of Pro4 of peptoid (0.31 nm) and other between main chain oxygen atom and side chain nitrogen atom of Lys3 of peptoid (0.22 nm) as shown in Fig. 8a. Six residues of $A\beta_{42}$ monomer (Asp1, Ala2, Glu3, His6, Gly9 and Tyr10) showed hydrophobic interactions with SLKP peptoid (Fig. 8b).

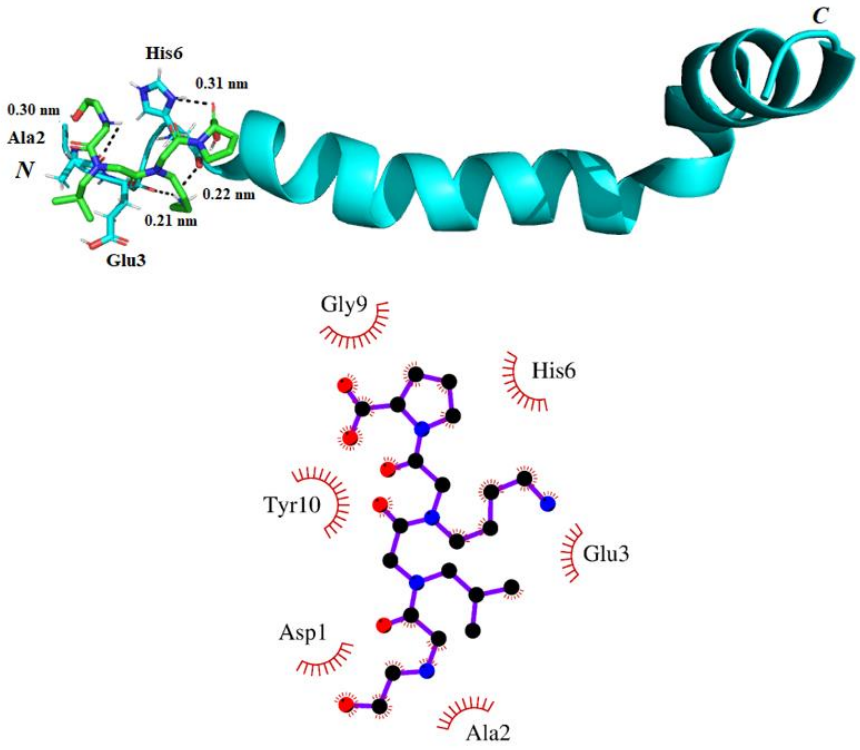

Figure 8: Docking pose of $A\beta_{42}$ monomer (PDB ID 1IYT) with SLKP peptoid showing hydrogen bonding interaction in (upper panel) and various hydrophobic interaction observed between $A\beta_{42}$ monomer and SLKP are shown in (lower panel) respectively.

The summary of molecular docking interaction of SLKP with $A\beta_{42}$ monomer is shown in Table 2.

Substrate	AutoDock Binding energy (kcal/mol)	Residue involved in hydrophobic interactions	Residues participating in intermolecular hydrogen bonds with SLKP		
			Residue of and atom of $A\beta_{42}$ monomer	Residue and atom of SLKP	Distance of hydrogen bonds
$A\beta_{42}$ monomer	-4.4	Asp1, Ala2, Glu3, His6, Gly9, Tyr10	Ala2 (O)	Ser1(N)	0.30 nm
			Glu3 (O)	Lys3(ND1)	0.21 nm
			His6 (O)	Lys3(ND1)	0.22 nm
			His6 (ND1)	Pro4(O)	0.31 nm

Table 2: Molecular docking analysis of $A\beta_{42}$ monomer with SLKP. Binding energy was calculated using Autodock-Vina.

6.2 Results of Molecular Dynamics (MD) Simulations

6.2.1 Comparison of simulation data with the experimental NMR observables

To access the ability of conformational ensemble generated of Aβ$_{42}$ monomer by MD we compare two type of NMR observables, chemical shift values and the scalar NH-Hα coupling values with the experimental data. [41], [42]. To evaluate the chemical shift data, we calculate the NMR chemical shift value for Cα and Cβ atoms using ShiftX2 program. [43] The values obtained for the Cα (R = 0.96), and Cβ (R = 0.77) nuclei shows close resemblance with the experimental NMR chemical shift values as shown in (Fig. 9a-b).

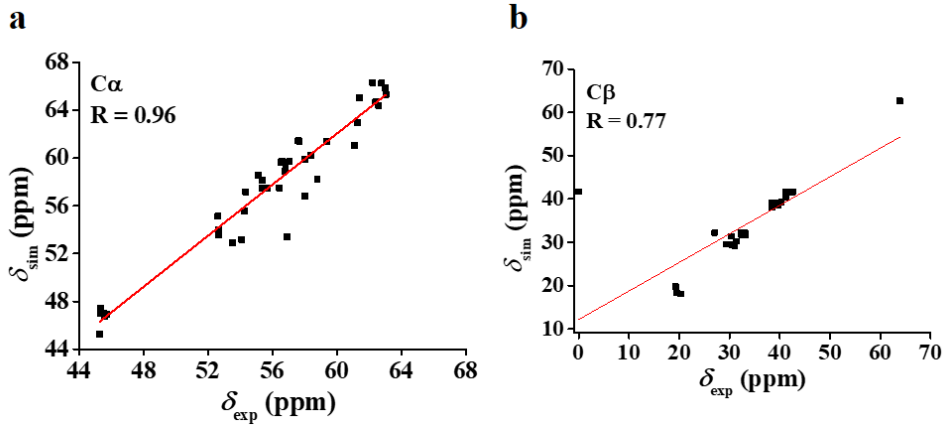

Figure 9: Correlation between theoretical and experimental NMR chemical shifts for Cα, Cβ atoms of Aβ$_{42}$ monomer as shown in panel a and panel b respectively.

Next, the ensembles generated of Aβ$_{42}$ monomer were evaluated for the scalar *J*–coupling ($^3J_{NH\text{-}H\alpha}$) constants and were calculated *via* the Karplus equation. The $^3J_{NH\text{-}H\alpha}$ coupling constant were obtained from the dihedral angles ϕ and ψ and Vuister and Bax parameters [44] were used in the Karplus equation[45] to obtain the value of $^3J_{NH\text{-}H\alpha}$ constants. The mean value of simulated $^3J_{HNH\alpha}$ constants for Aβ$_{42}$ monomer structure shows ~7.7 Hz, however the experimental value of $^3J_{HN\text{-}H\alpha}$ coupling constant is ~6.8 Hz. For the $^3J_{HN\text{-}H\alpha}$ coupling constants there is good correspondence between simulated and experimental coupling constant values. In literature study reported by Ball et al. shows near about same value of average $^3J_{HN\text{-}H\alpha}$ coupling constants exhibiting the ~7.6 Hz.[46]

Thus, the conformations obtained in performed simulation by using GROMOS force field shows good agreement with the experimental study.

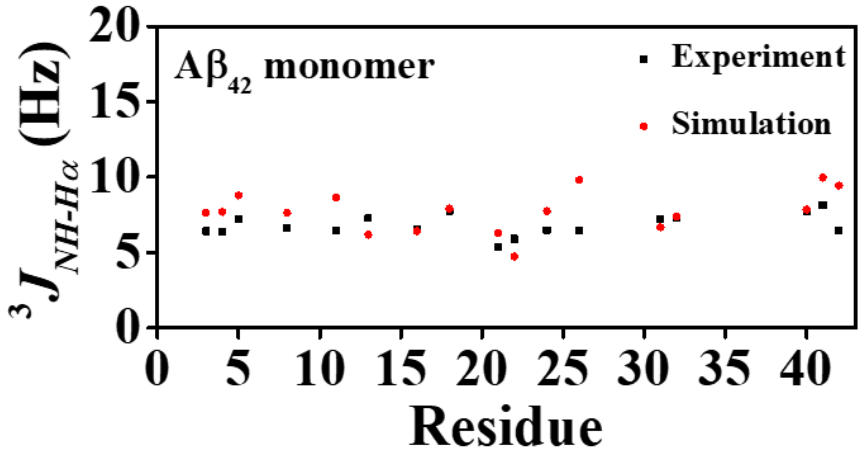

Figure 10: Comparison of simulated $^{3}J_{HN\text{-}H\alpha}$ coupling constants for the $A\beta_{42}$ monomer residues (red) with experimental measurements (black) published by Hou and co-workers.

6.2.2 Structural stability of $A\beta_{42}$ monomer in presence and absence of SLKP

In order to examine the relative conformational stability of $A\beta_{42}$ monomer and $A\beta_{42}$ monomer-SLKP complex, RMSD, R_g and RMSF were evaluated (Fig. 11). For $A\beta_{42}$ monomer, RMSD fluctuates to higher value (~1.2 nm) till the finish of simulation while for $A\beta_{42}$ monomer-SLKP complex, RMSD shows appreciably lower average fluctuation value of (~ 0.98 nm) as shown in Fig. 11a. The RMSD data depicts that SLKP complex stabilizes the structure of $A\beta_{42}$ monomer. Next the R_g of $A\beta_{42}$ monomer, $A\beta_{42}$ monomer-SLKP complex was calculated. The value of R_g for $A\beta_{42}$ monomer stays between 1.0-1.6 nm showing average value of 1.06 nm. However, in $A\beta_{42}$ monomer-SLKP complex the R_g shows lower mean value ~ 1.0 nm as shown in Fig. 11b which indicates that in presence of SLKP, the compactness of $A\beta_{42}$ monomer increases and hence becomes more stable.

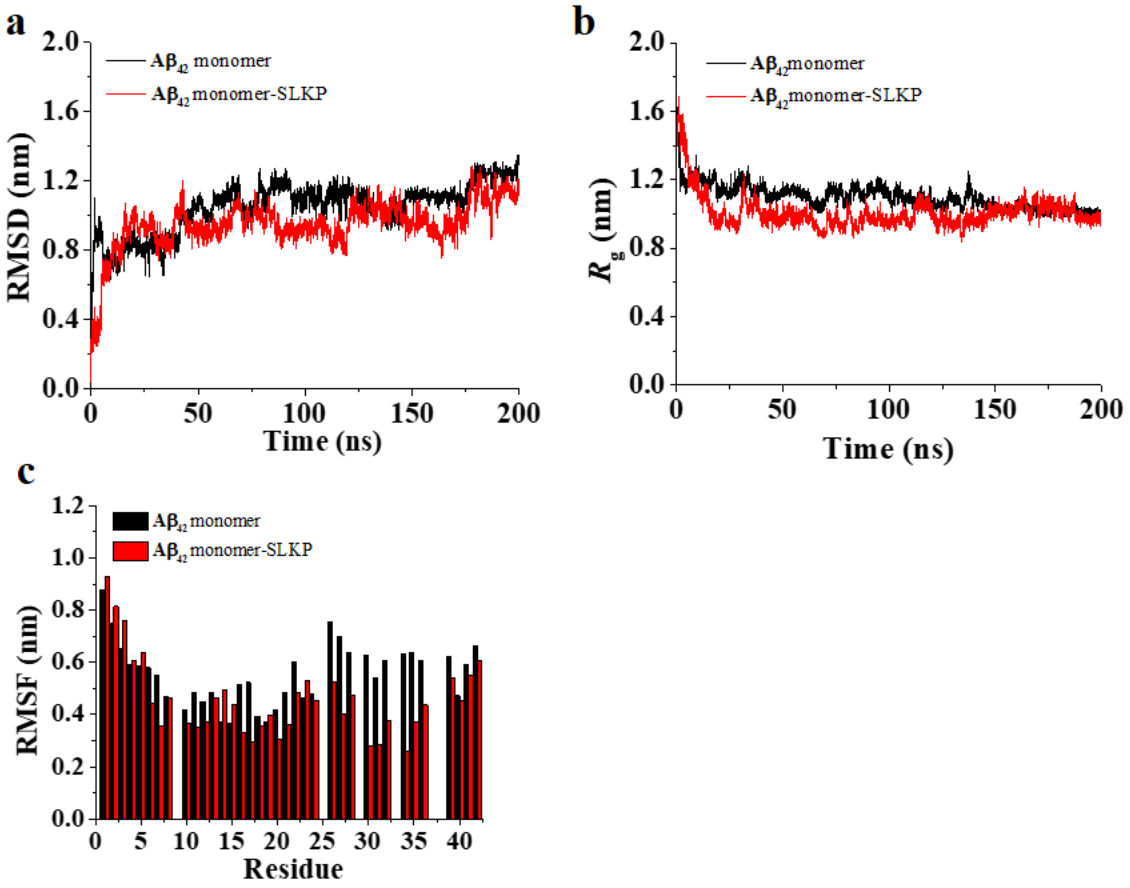

Figure 11: The RMSD (panel a) and R_g (panel b) are plotted as a function of simulation time in ns. RMSF of each residue in $A\beta_{42}$ monomer and $A\beta_{42}$ monomer-SLKP complex is shown in (panel c).

To observe the residue-vise fluctuations RMSF of side chain of each residue of $A\beta_{42}$ monomer and $A\beta_{42}$ monomer-SLKP complex was calculated. It is depicted in the Fig.11c that the residues in CHC and C-termini show less atomic fluctuations in $A\beta_{42}$ monomer-SLKP complex as compared to $A\beta_{42}$ monomer. The declined fluctuations of these residues in $A\beta_{42}$ monomer-SLKP complex illustrate the increased stability of the CHC and C-termini regions as compared to $A\beta_{42}$ monomer.

6.2.3 Clustering analysis of $A\beta_{42}$ monomer and $A\beta_{42}$ monomer-SLKP complex

The thermodynamic stability of the conformational ensemble of $A\beta_{42}$ monomer and $A\beta_{42}$ monomer-SLKP complex was assessed using cluster analysis. The indicative structures of the five most-populated microstates for $A\beta_{42}$ monomer and $A\beta_{42}$ monomer-SLKP peptoid complex as displayed in Fig. 12 and the population distribution of microstates are listed in Table 3.

System	No of microstates	Percentage population of five most-populated microstates				
		m_1	**m_2**	**m_3**	**m_4**	**m_5**
$A\beta_{42}$ monomer	86	30.1	18.9	15.6	5.8	3.7
$A\beta_{42}$ monomer-SLKP	62	33.7	24.5	16.3	6.0	3.9

Table 3: The total number of microstates and percent population of five most-populated microstates (m1, m2, m3, m4 and m5) for $A\beta_{42}$ monomer and $A\beta_{42}$ monomer-SLKP complex.

A lower number of conformational clusters observed for $A\beta_{42}$ monomer-SLKP in comparison to $A\beta_{42}$ monomer indicate lower conformational heterogeneity in $A\beta_{42}$ monomer-SLKP. The population of the most-populated microstate increases from 30.1% for $A\beta_{42}$ monomer to 33.7% for $A\beta_{42}$ monomer-SLKP (Table 3). The percentage population of next four most-populated microstates increases from 18.9%, 15.6%, 5.8%, and 3.7% in $A\beta_{42}$ monomer to 24.4%, 16.3%, 6.0%, and 3.9% in $A\beta_{42}$ monomer-SLKP, which highlight less heterogeneous conformational ensemble for $A\beta_{42}$ monomer-SLKP. The top five microstates of $A\beta_{42}$ monomer and $A\beta_{42}$ monomer-SLKP complex comprises 66.1% and 84.4% of the total conformational ensemble, respectively. Out of five most-populated microstates of $A\beta_{42}$ monomer m2, m4 and m5 have shown β-sheet conformation at C-terminal whereas in case of $A\beta_{42}$ monomer-SLKP complex these microstates have adopted helical conformation. The preservation of helix conformation and loss of β–sheet conformation in presence of SLKP shows prevention of conformational transition in $A\beta_{42}$ monomer.

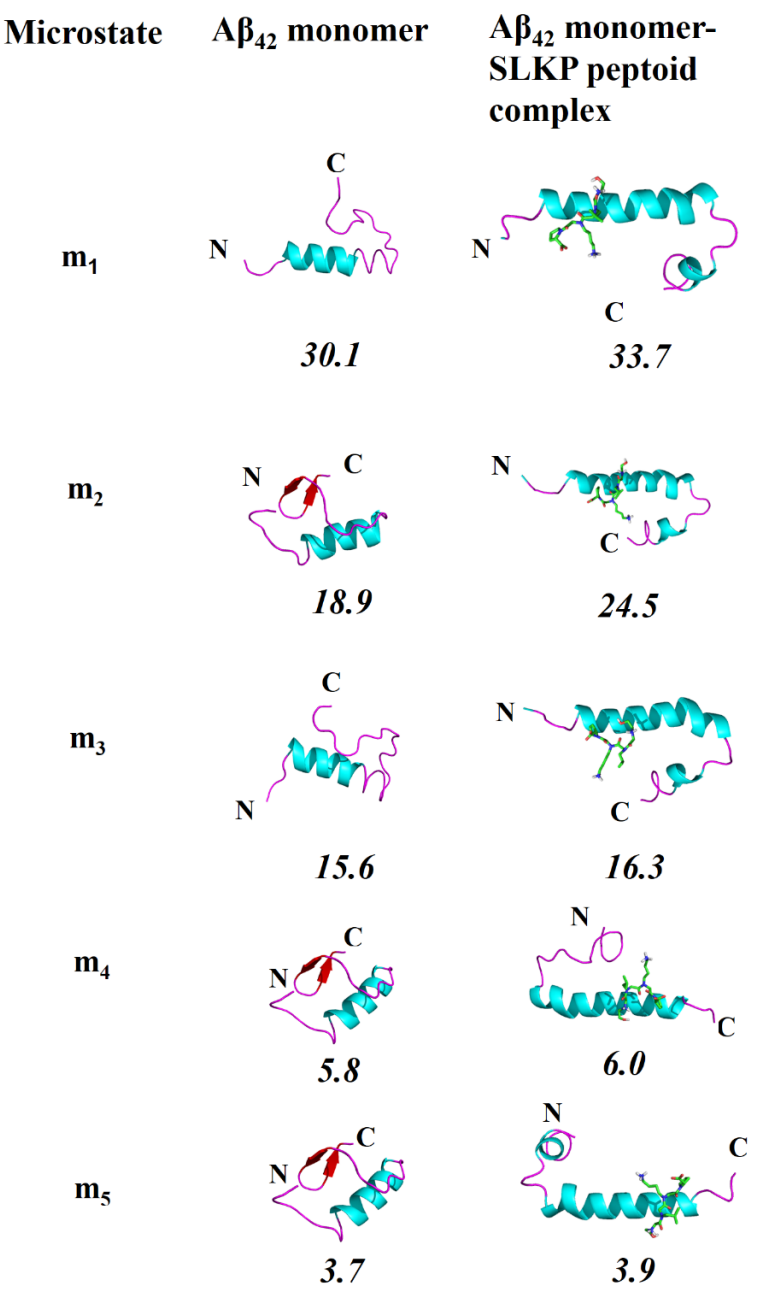

Figure 12: The representative member of the five most-populated microstates (**m**$_1$, **m**$_2$, **m**$_3$, **m**$_4$ and **m**$_5$) of Aβ$_{42}$ monomer and Aβ$_{42}$ monomer-SLKP complex. The percentage population of each microstate is shown underneath cartoon models. The Aβ$_{42}$ monomer is shown as a cartoon representation with N- and C-termini labeled and SLKP is shown in stick representation.

6.2.4 Overall and per-residue secondary structure analysis of $A\beta_{42}$ monomer and $A\beta_{42}$ monomer-SLKP complex

To monitor the changes in conformation in $A\beta_{42}$ monomer and $A\beta_{42}$ monomer-SLKP during simulation, the time evolution of secondary structures were computed using DSSP method. The secondary structure depictions of $A\beta_{42}$ monomer and $A\beta_{42}$ monomer-SLKP peptoid complex while simulation are displayed in Fig. 13.

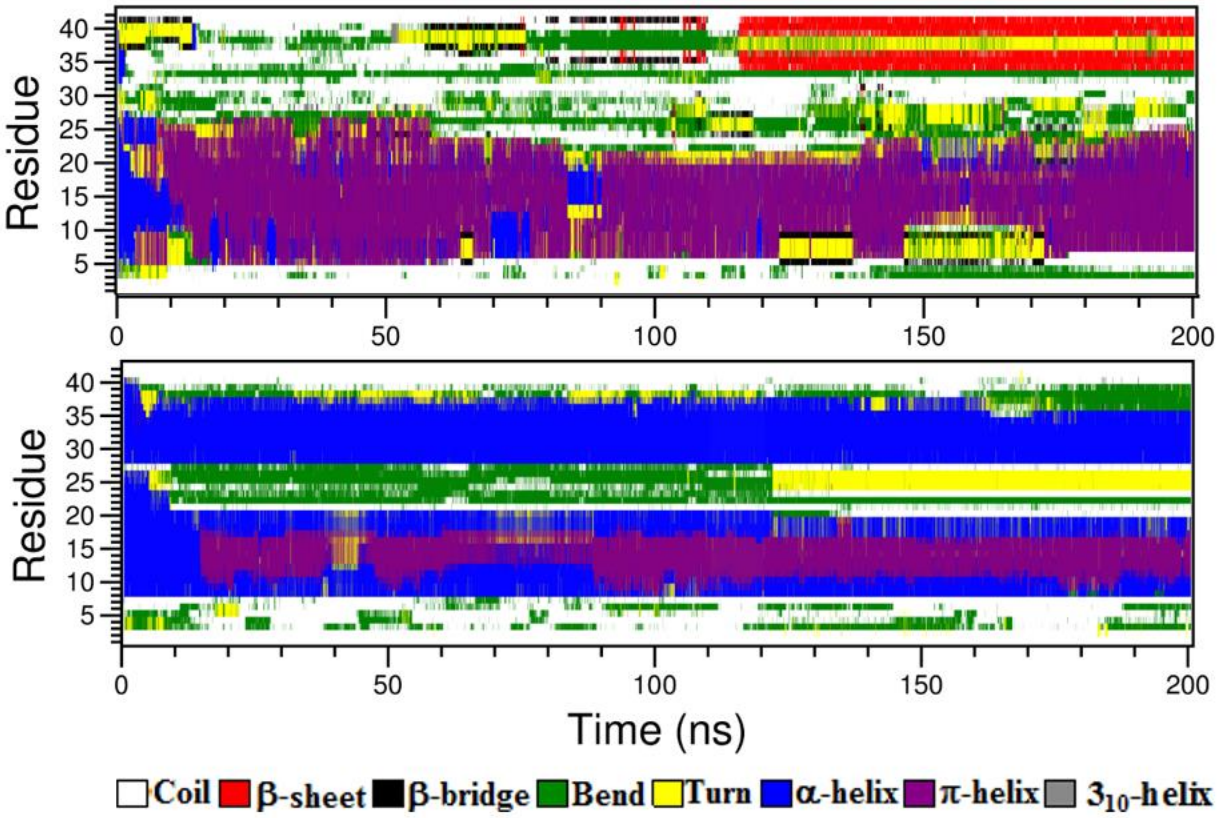

Figure 13: The evolution of secondary structure for $A\beta_{42}$ monomer (upper panel) and $A\beta_{42}$ monomer-SLKP complex (lower panel) evaluated using dictionary of secondary structure of proteins (DSSP) in water. The Y-axis represents residues of $A\beta_{42}$ monomer and X-axis represents simulation time in ns. The secondary structure of $A\beta_{42}$ is color-coded as shown underneath.

For $A\beta_{42}$ monomer, π–helix is dominant (30%), followed by random coil (29%) conformation (Table 4). The population of bend, turn, β-content and α–helix conformations are 14%, 12%, 10% and 5% respectively, as shown in Table 4. The β-content in $A\beta_{42}$ monomer is dominantly

populated at C-terminal after 120 ns simulation whereas α–helix is preserved in N-terminal till 10 ns simulation only as shown in upper panel Fig. 13.

Model system	coil	β-sheet[a]	Bend	Turn	Helix[b]
$A\beta_{42}$ monomer	29	10	14	12	35
$A\beta_{42}$ monomer-SLKP	28	1	12	7	51

[a]β-sheet is the sum of β-sheet and β-bridge; [b]helix is the sum of α–, π–, and 3_{10} helix

Table 4: The secondary structural component statistics percentage of $A\beta_{42}$ monomer and $A\beta_{42}$ monomer-SLKP complex during molecular dynamics simulation in water as explicit-solvent.

To study the impact of SLKP on secondary structure inclination of $A\beta_{42}$ monomer, time evolution of secondary structure analysis for $A\beta_{42}$ monomer-SLKP complex was carried out. In presence of SLKP, the percentage of α–helix significantly increases from 5% to 37% whereas the percentage of β-sheet abruptly decreases from 10% to 1% (Table 4). The α–helix conformation is highly preserved in $A\beta_{42}$ monomer-SLKP complex while simulation. The α–helix content, random coil and bend conformations were observed at N- and C-terminal of $A\beta_{42}$ monomer-SLKP peptoid complex as shown in lower panel (Fig. 13). The concomitant increment in α–helix and significant decrement in β-content in presence of SLKP clearly indicates the potential of SLKP to inhibit amyloid aggregation.

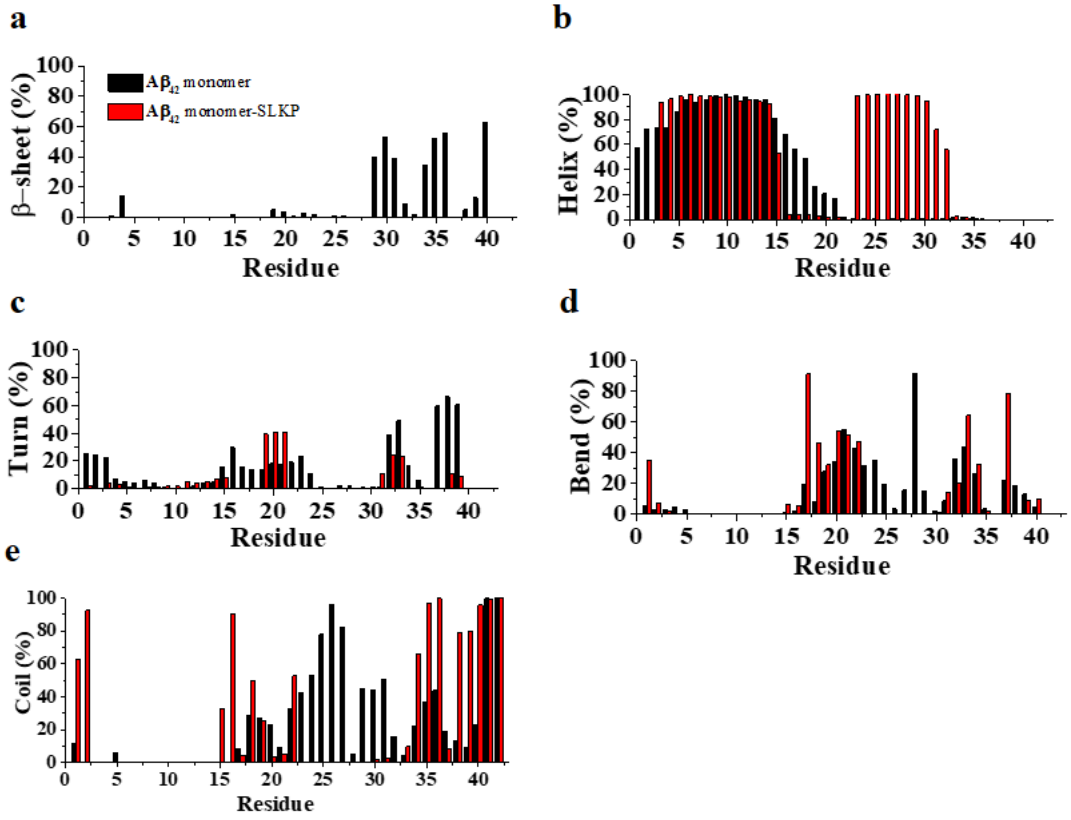

Figure 14: The per-residue secondary structure components of β-sheet (panel a), Helix (panel b), Turn (panel c), Bend (panel d) and Coil (panel e) of $A\beta_{42}$ monomer (black) and $A\beta_{42}$ monomer-SLKP complex (red).

The per-residue secondary structure analysis demonstrated remarkably lowered β-sheet aggregation in $A\beta_{42}$ monomer-SLKP complex. The aggregation vulnerable β-sheet conformation was discerned in Phe4, Gly29-Met35 and Val39, Val40 which are CHC, N- and C-termini residues of $A\beta_{42}$ monomer (Fig. 14a) while no β-sheet was detected in presence of SLKP.

Remarkably intensified prospect of helix conformation from ~45% to ~98% of residues of $A\beta_{42}$ monomer in presence of SLKP is shown in Fig.14b. About 20 residues located in Asp1–Phe20 regions have proclivity to acquire helical conformation in $A\beta_{42}$ monomer, while a relatively larger number of residues, ~28 relative to Glu3-Val18 and Asp23-Gly33 regions, acquire helical conformation in $A\beta_{42}$ monomer-SLKP complex (Figure 14b). The increased content of helical conformation in key N- terminal and CHC region Glu3-Val18 and Asp23-Gly33 residues in

presence of SKLP as compare to $A\beta_{42}$ monomer (Fig. 14b) demonstrates stabilization of $A\beta_{42}$ monomer native conformation.

The residues opting turn conformation showed remarkable decrement from 26 residues located in Asp1-Ser8, Gln15-Val24, Ile31-Met35, Gly37-Val39 regions of $A\beta_{42}$ monomer to half ~13 (Asp1, Ala2, Gln15-Glu22, Ile31-Gly33, Gly38, Val39) of $A\beta_{42}$ monomer-SLKP complex (Fig. 14c). Ono et al., revealed the significance of Ser8 andGly9 residues in the turn conformation. He proposed that turn conformation permits N-terminal region to interconnect with CHC region and impact the Aβ aggregation[47]. A remarkable decrement in turn conformation was seen for Ser8 and Gly9 residues in presence of SLKP (Fig. 14c).

The residues opting bend conformation also displayed notable decrement from 23 residues located in Asp1, Ala2, Lys16-Gly29, Ile31-Leu34, Gly37-Val39 regions of $A\beta_{42}$ monomer to only 15 (Glu11-Gln15, Phe19-Ala21, Ile31-Gly33, Ile31-Leu34, Gly37, Val39, Val40) of $A\beta_{42}$ monomer-SLKP complex (Fig. 14d).

About ~29 residues (Asp1, Arg5, Lys16-Ala42) for $A\beta_{42}$ monomer and 21 residues (Asp1, Ala2, Gln15-Glu22, Ala30, Gly33-Ala42) for $A\beta_{42}$ monomer-SLKP complex opted coil conformation (Fig. 14e). $A\beta_{42}$ monomer-SLKP complex showcase decreased likelihood for coil conformation in turn region (24-30), which, thusly, prompts lower conformational flexibility in $A\beta_{42}$ monomer in presence of SLKP.

6.2.5 Salt bridge analysis and tertiary contact map of $A\beta_{42}$ monomer and $A\beta_{42}$ monomer–SLKP complex

It has been reported that the salt bridge interaction between Asp23 and Lys28 in $A\beta_{42}$ monomer plays an important role in fibril formation[48]. Hence the likelihood of Asp23–Lys28 salt bridge formation in $A\beta_{42}$ monomer and $A\beta_{42}$ monomer–SLKP complex was inspected to assess the impact of SLKP on $A\beta_{42}$ monomer accretion as shown in Fig. 15.

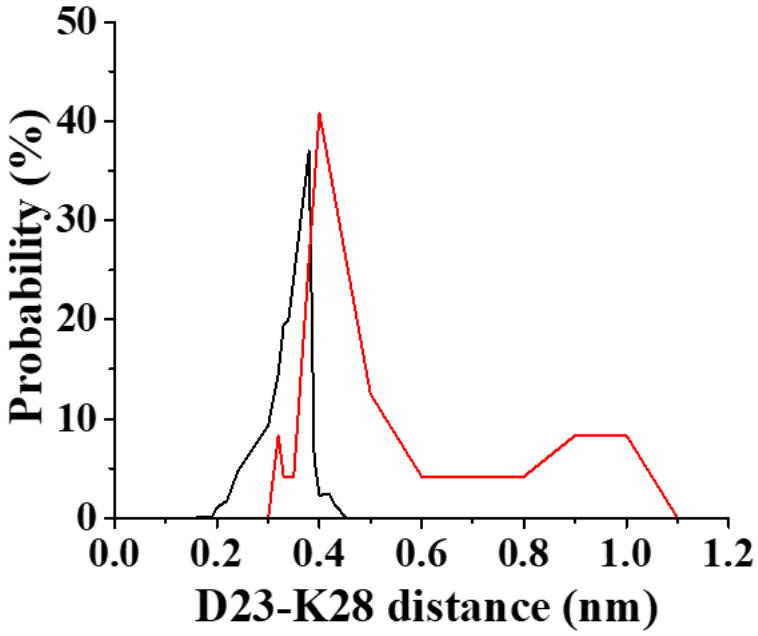

Figure 15: The distance distributions between Asp23 and Lys28 residues for salt bridge formation in the $A\beta_{42}$ monomer (black) and $A\beta_{42}$ monomer-SLKP peptoid complex (red).

According to literature the distance between two partaking charged residues should be ~ 0.46 nm for salt bridge formation.[49] In case of $A\beta_{42}$ monomer, a distance peak at ~0.40nm shows Asp23–Lys28 salt bridge formation (Fig. 15). In case of $A\beta_{42}$ monomer–SLKP complex, the probability distribution of salt bridge becomes broader and shifts to higher distance range. Thus, $A\beta_{42}$ monomer–SLKP complex shows destabilized Asp23–Lys28 salt bridge interaction, which features lower likelihood of development of bend which thusly decreases the aggregation inclination of $A\beta_{42}$ monomer in presence of SLKP.

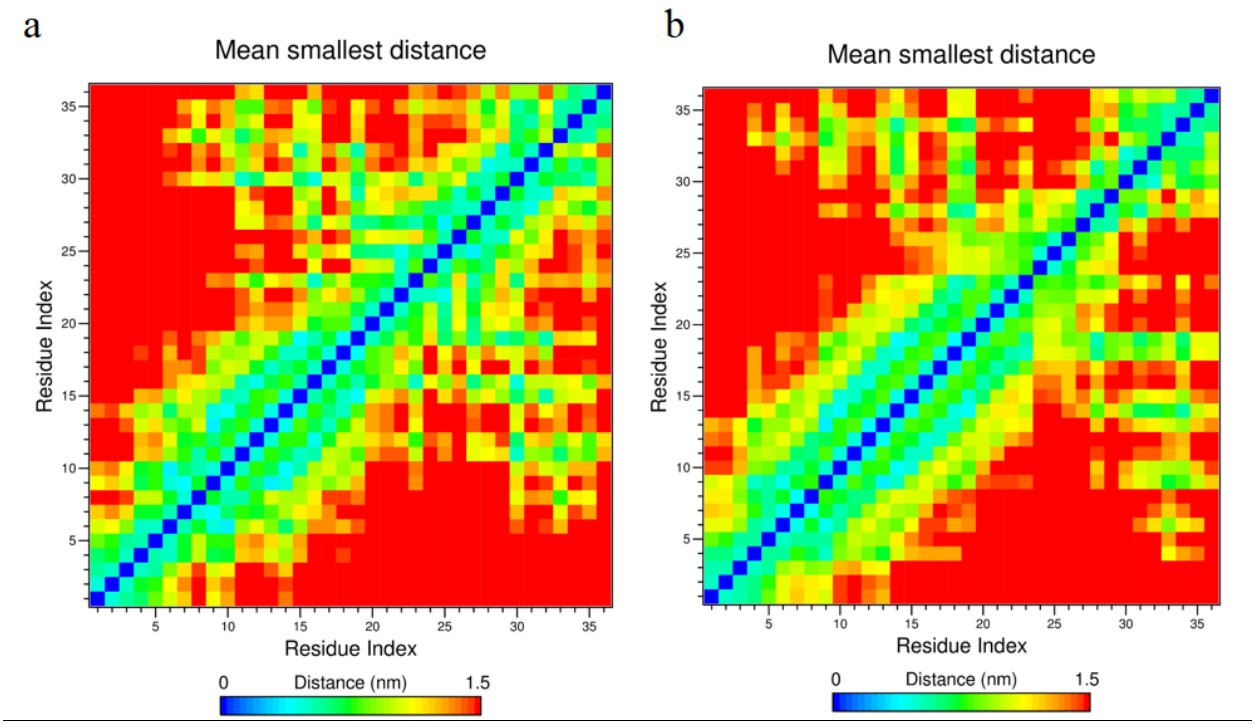

Figure 16: The residue-residue contact maps between $A\beta_{42}$ monomer (panel a**)** and $A\beta_{42}$-SLKP complex (panel b). The cut-off distance between atoms used to define contact is 1.5 nm.

Many experimental and theoretical studies have shown that the interaction between CHC and C-terminal region have prominent role in early $A\beta_{42}$ folding and self-assembly[50]. It has also been in literature that increase in intra-molecular interactions between CHC and C-terminal region promotes folding and self-aggregation process[51]. Here in case of $A\beta_{42}$ monomer, it was observed that the interactions were short range between CHC and C- terminal region (within 1.5 nm distance between side chain atoms) as shown in Fig. 16a whereas in case of $A\beta_{42}$ monomer–SLKP complex, it was found that there was decrease in intra-molecular tertiary contacts between CHC and C-terminus (Fig. 16b). These results depicted that in presence of SLKP, there was reduction in intra-peptide contacts which reduces the probability of $A\beta_{42}$ folding and self-aggregation.

6.2.6 Review of molecular interactions between $A\beta_{42}$ monomer and SLKP by utilizing binding free energy analysis

To review the molecular interactions between $A\beta_{42}$ monomer and SLKP, binding free energy analysis for $A\beta_{42}$ monomer–SLKP complex was assessed utilizing MM-PBSA approach.

Energy terms (kcal/mol)	$A\beta_{42}$ monomer-SLKP
ΔE_{vdW}	–43.5 ± 0.34
ΔE_{elec}	–9.8 ± 0.21
$\Delta E_{MM}{}^{a}$	–53.3 ± 0.55
ΔG_{ps}	19.7 ± 0.03
ΔG_{nps}	–7.4 ± 0.32
$\Delta G_{solv}{}^{b}$	12.3 ± 0.35
$\Delta G_{binding}{}^{c}$	–40.5 ± 0.90

$^{a}\Delta E_{MM} = \Delta E_{vdW} + \Delta E_{elec}$; $^{b}\Delta G_{solv} = \Delta E_{ps} + \Delta E_{nps}$; $^{c}\Delta G_{binding} = \Delta E_{MM} + \Delta G_{solv}$

Table 5: The binding free energy (kcal/mol) between $A\beta_{42}$ monomer and SLKP calculated by MM-PBSA.

SLKP binds with $A\beta_{42}$ monomer with a favorable binding energy (-40.5 kcal/mol). As reported from data in Table 5, non-polar van der Waals (ΔE_{vdw} = -43.5 kcal/mol) and polar electrostatic (ΔE_{elec} = -9.8 kcal/mol) interactions are ideal for $A\beta_{42}$ monomer–SLKP complex. The non-polar (ΔG_{nps} = -7.4 kcal/mol) contribution dominate over polar (ΔG_{ps} = 19.7 kcal/mol) and give most to solvation term.

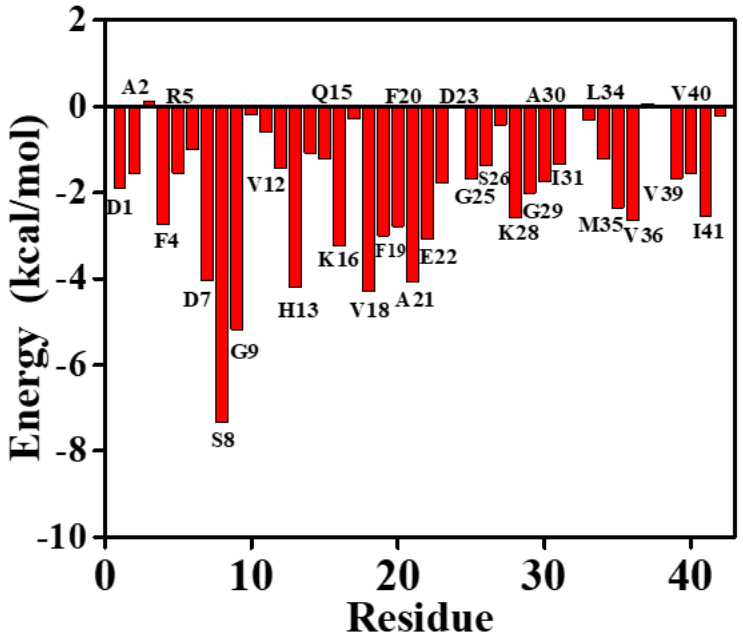

Figure 17: The binding free energy (kcal/mol) contribution of each residue of $A\beta_{42}$ monomer in $A\beta_{42}$ monomer–SLKP complex.

Further $A\beta_{42}$ monomer's each residue contribution to the binding free energy in $A\beta_{42}$ monomer-SLKP complex was assessed.[52] Those residues which are having interaction energy less than -1 kcal/mol with the substrate are marked as significant (*i.e.* they are marked as hot residues)[53]. As depicted in Fig. 17, Asp1, Ala2, Phe4, Arg5, Lys7, Ser8, Gly9, Val12, His13, Gln15, Lys16, Val18, Phe19, Phe20, Ala21, E22, D23, Gly25, Ser26, Lys28, Gly29, Ala30, Ile31, Leu34, Met35, Val36, Val39, Val40, Ile41 are hot residues for $A\beta_{42}$ monomer and SLKP binding. The residues Asp7, Ser8, Gly9, His13, Val18 and Ala21 have topmost participation in the binding energy (Fig. 17). Moreover SLKP binds firmly with Lys 16 and Lys 28 which play an expository part in $A\beta_{42}$ accretion. The results of MM-PBSA confirms strong binding and high spots the part played by important amino acids in binding of SLKP and $A\beta_{42}$ monomer.

6.2.7 Free energy landscape (FEL) of $A\beta_{42}$ monomer and $A\beta_{42}$ monomer–SLKP complex

The FEL was plotted to get an understanding of conformational states related with different free energy states. The FEL was plotted for $A\beta_{42}$ monomer and $A\beta_{42}$ monomer–SLKP complex utilizing the first two PCs (PC1 and PC2).

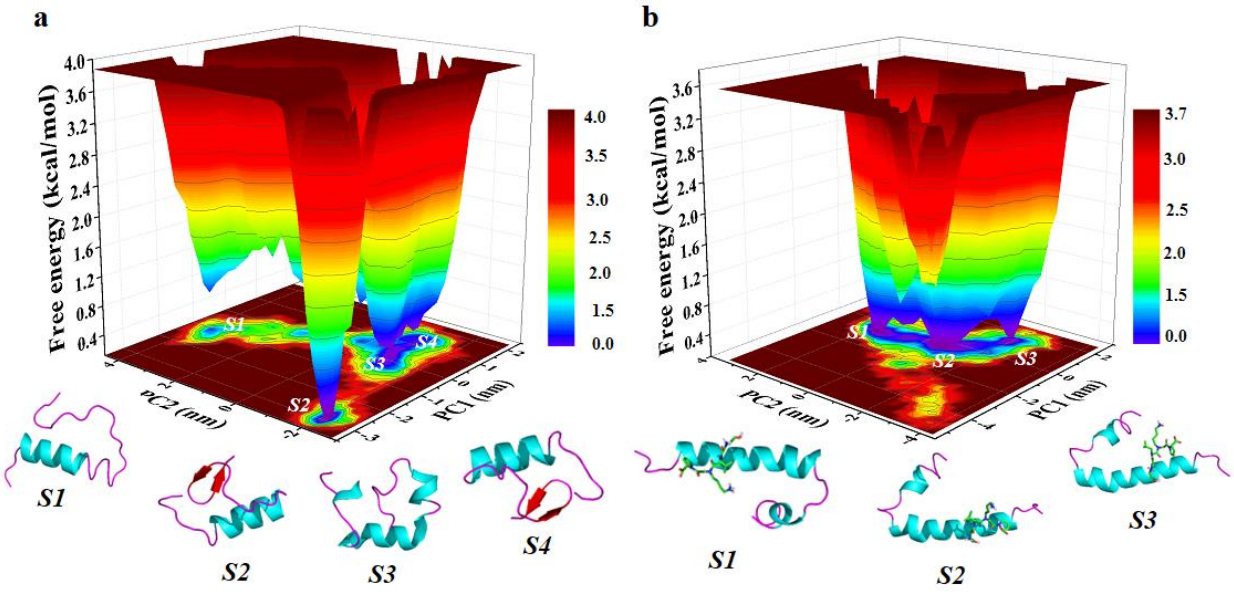

Figure 18: FEL generated by projecting first two principal components, PC1, and PC2, are shown for $A\beta_{42}$ monomer and $A\beta_{42}$ monomer-SLKP complex in panel a, and b, respectively. The conformational distribution is shown in the colored region in FEL. The red region depicts conformations having high energy, while blue corresponds to conformations with lower energy.

The FEL of $A\beta_{42}$ monomer delineate various metastable states which are connected through energy barriers and contain four recognizable minimum energy basins related with its conformational states (Fig. 18a). The blue region portrays free energy minima, cyan and green regions signify meta-stable conformational states. Comparatively $A\beta_{42}$ monomer–SLKP complex has three predominant minimum energy basin related with the most reduced energy conformational state (Fig. 18b).

7. Conclusion

In the present study, the impact of SLKP peptoid on structural stability of $A\beta_{42}$ monomer was probed using computational techniques. MD simulations reveal that SLKP peptoid remarkably inhibits conformational transformation of helical conformation to β-sheet conformation which is prone to aggregation in $A\beta_{42}$ monomer. The molecular docking and MM-PBSA revealed that SLKP peptoid preferentially binds at N-terminal region of $A\beta_{42}$ monomer. MD simulation analysis highlights various important points such as: *i*) SLKP prevents conformational transformation of $A\beta_{42}$ monomer by stabilizing native helical conformation as demonstrated by conformational clustering, DSSP and per residue secondary structure analysis; *ii*) SLKP prevents amyloid aggregation by destabilizing D23-K28 salt bridge interaction which is responsible for formation of bend which helps in self-aggregation in $A\beta_{42}$ monomer; *iii*) Tertiary contact map analysis highlights the reduction of intra-peptide contacts in presence of SLKP which are responsible for aggregation of $A\beta_{42}$ monomer structure; *iv*) The representative conformations discovered by clustering method and FEL analysis reveal the presence of aggregation–prone β–sheet conformation in $A\beta_{42}$ monomer, whereas the most–dominant conformations of $A\beta_{42}$ monomer–SLKP complex exist in native helical or random coil structure.

The results of present study furnished significant information about the obstructing mechanism of SLKP against $A\beta_{42}$ aggregation that will further help to design new peptidomimetic drugs to target $A\beta_{42}$ monomer aggregation which may become potential therapeutics against AD.

8. References

1. https://www.niehs.nih.gov/research/supported/health/neurodegenerative/index.cfm

2. https://www.alz.co.uk/research/WorldAlzheimerReport2018.pdf

3. Lane, C. A.; Hardy, J.; Schott, J. M. Alzheimer's disease. *Eur. J. Neurol.,* **2018**, *25*, 59-70.

4. Wong, C. W.; Quaranta, V.; Glenner, G. G. Neuritec plaques and cerebrovascular amyloid in Alzheimer's disease. *Proc. Natl. Acad. Sci. USA* **1985**, *82*, 8723-8732.

5. Pradhan, K., Das, G., Gupta, V., Mondal, V., Barman, S., Khan, J., Ghosh, S. Discovery of neuroregenerative peptoid from amphibian neuropeptide that inhibits amyloid-β toxicity and crosses blood-brain barrier. *ACS Chem. Neurosci.* **2019**, *10*, 1355-1368.

6. Ritchie, C.W.; Bush, A. I.; Mackinnon, A.; Macfarlane, S.; Mastwyk, M.; MacGregor, L.; Kiers, L.; Cherny, R.; Li, Q. X.; Tammer, A.; Carrington, D.; Mavros, C.; Volitakis, I.; Xilinas, M.; Ames, D.; Davis, S.; Beyreuther, K.; Tanzi. R. E.; Masters, C.L. Metal-protein attenuation with iodochlorhydroxyquin (clioquinol) targeting Aβeta amyloid deposition and toxicity in Alzheimer disease: a pilot phase 2 clinical trial. *Arch. Neurol*. **2003**, *60*, 1685-1691.

7. Ritchie, C.W.; Bush, A. I.; Masters, C. L. Metal-protein attenuating compounds and Alzheimer's disease. *Expert Opin. Investig. Drugs* **2004**, *13*, 1585-92.

8. Wood, S. J.; MacKenzie, L.; Maleeff, B.; Hurle, M. R.; Wetzel, R. Selective inhibition of Aβeta fibril formation. *J. Biol. Chem. A* **1996**, *271*, 4086-92.

9. Barale, S. S.; Parulekar, R. S.; Fandilolu, P. M.; Dhanavade, M. J.; Sonawane, K. D. Molecular insights into destabilization of Alzheimer's Aβ protofibril by arginine containing short peptides: a molecular modelling approach. *ACS Omega* **2019**, *4*, 892−903.

10. Viet, M.H.; Ngo, S. T.; Lam, N. S.; Li, M. S. Inhibition of aggregation of amyloid peptides by beta-sheet breaker peptides and their binding affinity. *J. Phys. Chem. B* **2011**, *115*, 7433-7446.

11. Jagota, S.; Rajadas, J. Synthesis of D-amino acid peptides and their effect on beta-amyloid aggregation and toxicity in transgenic Caenorhabditis elegans. *Med. Chem. Res*. **2013,** *22*, 3991-4000.

12. Ashur-Fabian, O.; Segal-Rudera, Y.; Skutelskyb, E.; Brennemanc, D. E.; Steingarta, R. A.; Giladia, E.; Gozesa, I. The neuroprotective peptide NAP inhibits the aggregation of the beta-amyloid peptide. *Peptides* **2003**, *24*, 1413-1423.

13. Granica, I.; Masmana, M. F.; Muldera, C. K.; Nijholta,b, I. M.; Naudea,c , P. J. W.; de Haana, A.; Em¨oke Borb´elyd.; Penked, B.; Luitena,c; P.G.M.; Eisela, U. L. M. LPYFD Neutralizes amyloid-β-induced memory impairment and toxicity. *J. Alzheimers Dis*. **2010**, *19*, 991-1005.

14. Neddenriep, B.; Calciano, A.; Conti, D.; Sauve, E.; Paterson, M.; Bruno, E.; Moffet, D. A. Short peptides as inhibitors of amyloid aggregation. *Open Biotechnol. J.* 2011, *5,* 39-46.

15. Gilman, S.; Koller, M.; Black, R. S.; Jenkins, L.; Griffith, S. G.; Fox, N. C.; Eisner, L.; Kirby, L., Rovira; M. B.; Forette, F.; Orgogozo, J. M. Clinical effects of Abeta immunization (AN1792) in patients with AD in an interrupted trial. *Neurology* **2005**, *64*, 1553-1562.

16. Karran, E.; Mercken, M.; De Strooper, B. The amyloid cascade hypothesis for Alzheimer's disease: an appraisal for the development of therapeutics. *Nat. Rev. Drug Discovery* **2011,** *10,* 698−712.

17. Amijee, H.; Scopes, D. I. The quest for small molecules as amyloid inhibiting therapies for Alzheimer's disease. *J. Alzheimer's Dis.* **2009**, *17*, 33−47.

18. Mehrazma, B.; Rauk, A. Exploring amyloid-beta dimer structure using molecular dynamics simulations. *J. Phys. Chem. A* **2019**, *22*, 4658-4670.

19. Young, S. C. A systematic review of antiamyloidogenic and metal-chelating peptoids: two structural motifs for the treatment of Alzheimer's disease. *Molecules* **2018**, *23*, 296, DOI: 10.3390/molecules23020296.

20. Baig, M. H.; Ahmad, K.; Rabbani, G.; Choi, I. Use of peptides for the management of Alzheimer's disease: diagnosis and inhibition. *Front. Aging Neurosci.* **2018**, DOI: 10.3389/fnagi.2018.00021.

21. Chiti, F.; Dobson, C. M. Protein misfolding, amyloid formation and human disease: a summary of progress over the last decade. *Annu. Rev. Biochem.* **2017**, *86*, 27-68.

22. Soto, C. Unfolding the role of Protein Misfolding in Neurodegenerative diseases. Nat. Rev. Neurosci. **2003**, *4*, 49-60.

23. Selkoe, D. J.; Hardy, J. The amyloid hypothesis of Alzheimer's disease at 25 years. *EMBO Mol. Med*. **2016**, *8*, 595-608.

24. Meng, X. Y.; Zhang, H. X.; Mezei, M.; Cui, M. Molecular docking: a powerful approach for structure-based drug discovery. *Curr. Comput. Aided Drug Des.* **2011**, *7*, 146-157.

25. Durrant, J. D.; McCammon, J. A. Molecuar dynamics simulations and drug discovery. *BMC. Biol.* **2011**, *9*, 71, DOI: 10.1186/1741-7007-9-71.

26. Saini, R. K.; Shuaib, S.; Goyal, D.; Goyal, B. Insights into the inhibitory mechanism of a resveratrol and clioquinol hybrid against Aβ42 aggregation and protofibril destabilization: a molecular dynamics simulation study. *J. Biomol. Struct. Dyn.* **2018**, 3183-3197, DOI: 10.1080/07391102.2018.1511475.

27. Shuaib, S.; Saini, R.K.; Goyal, D.; Goyal, B. Insights into the inhibitory mechanism of dicyanovinyl-substituted J147 derivative against Aβ42 aggregation and protofibril destabilization: A molecular dynamics simulation study. *ChemistrySelect* **2017**, *2*, 1645-1657.

28. Sharma, B.; Ranganathan, S. V.; Belfort, G. Weaker N-terminal interactions for the protective over the causative Aβ peptide dimer mutants. *ACS Chem. Neurosci.* **2018**, *6*, 1247-1253.

29. Nasica-Labouze, J.; Nguyen, P. H.; Sterpone, F.; Berthoumieu, O.; Buchete, N. V.; Coté, S.; De Simone, A.; Doig, A. J.; Faller, P.; Garcia, A.; Laio, A.; Mai, S. L.; Melchionna, S.; Mousseau, N.; Mu, Y.; Paravastu, A.; Pasquali, S.; Rosenman, D. J.; Strodel, B.; Tarus, B.; Viles, J. H.; Zhang,T.; Wang, C.; Derreumaux, P. Amyloid β protein and Alzheimer's disease: when computer simulations complement experimental studies. *Chem. Rev*. **2015**, *115*, 3518-3563.

30. Trott, O.; Olson, A. J. AutoDock Vina: Improving the speed and accuracy of docking with a new scoring function, efficient optimization, and multithreading. *J. Comput. Chem*. **2009**, DOI: 10.1002/jcc.21334.

31. Stroet, M.; Caron, B., Visscher, K.M.; Geerke, D. P.; Malde, A. K.; Mark, A. E. Automated topology builder version 3.0: prediction of solvation free enthalpies in water and hexane. *J. Chem. Theory Comput*. **2018**, *11*, 5834-5845.

32. Lindahl, E.; Hess, B.; van der Spoel, D. GROMACS 3.0: a package for molecular simulation and trajectory analysis. *J. Mol. Model.* **2001**, *7*, 306–317.

33. Abraham, M.J.; Murtola, T.; Schulz, R.; Pall, S.; Smith, J. C.; Hess, B.; Lindahl, E. GROMACS: high performance molecular simulations through multi-level parallelism from laptops to supercomputers. *Software X* **2015**, *2*, 19-25.

34. Hess, B.; Bekker, H.; Berendsen, H. J. C.; Fraaije, J. LINCS: a linear constraint solver for molecular simulations. *Comput. Chem.* **1997**, *18*, 1463-1472.

35. Bhavaraju, M.; Phillips, M.; Bowman, D.; Aceves-Hernandez, J. M.; Hansmann, U. H. E. Binding of ace-inhibitors to *in vitro* and patient derived amyloid-β fibril models. *J. Chem. Phys*. **2016**, DOI: 10.1063/1.4938261.

36. Berendsen, H. J. C.; Postma, J.P.M.; Gunsteren, W. F.; DiNola, A.; Haak, J. R. Molecular dynamics with coupling to an external bath. *J. Chem. Phys.* **1984**, *81*, 3684.

37. Humphrey, W.; Dalke, A.; Schulten, K. VMD: Visual molecular dynamics. *J. Mol. Graph.* **1996**, *14*, 33-38.

38. DeLano, W. L. The PyMOL Molecular Graphics System. *San Carlos, DeLano Scientific* **2002**.

39. Daura, X.; Gademann, K.; Jaun, B.; Seebach, D.; Gunsteren, W. F.; Mark, A. E. Peptide folding: when simulation meets experiment. *Angew. Chem. Int. Ed.* **1999**, *38*, 236-240.

40. Kabsch, W.; Sander, C. Dictionary of protein secondary structure: pat09ern recognition of hydrogen-bonded and geometrical features. *Biopolymers* **1983**, *12*, 2577-2637.

41. Hou, L.; Shao, H,; Zhang, Y.; Li, H.; Menon, N. K.; Neuhaus, E. B.; Brewer, J. M.; Byeon, In. Ja.; Ray, D. G.; Vitek, M. P.; Iwashita, T,; Makula, R. A.; Przybyla, A. B.; Zagorski, M. G. Solution NMR studies of the Aβ(1-40) and Aβ(1-42) peptides establish that the Met35 oxidation state affects the mechanism of amyloid formation. *J. Am. Chem. Soc.* **2004**, *126*, 1992−2005.

42. Paravastu, A. K.; Leapman, R.D.; Yau, W. M.; Tycko, R. Molecular structural basis for polymorphism in Alzheimer's β-amyloid fibrils. *Proc. Natl. Acad. Sci. USA* **2008**, *105*, 18349–18354.

43. Han, B.; Liu, Y.; Ginzinger, S. W.; Wishart, D. S. SHIFTX2: Significantly improved protein chemical shift prediction. *J. Biomol. NMR* **2011**, *50*, 43–57.

44. Vuister, G. W.; Bax, A. Quantitative J correlation: a new approach for measuring homonuclear three-bond J ($H^N H^\alpha$) coupling constants in ^{15}N-enriched proteins. *J. Am. Chem. Soc.* **1993**, *115*, 7772–7777.

45. Karplus, M. Contact electron–spin coupling of nuclear magnetic moments. *J. Chem. Phys*., **1959**, *30*, 11–15.

46. Ball, K. A.; Phillips, A. H.; Nerenberg, P. S,; Fawzi, N. L.; Wemmer, D. E.; Head-Gordon, T. Homogeneous and heterogeneous tertiary structure ensembles of amyloid-β peptides., *Biochemistry* **2011**, *50*, 7612–7628.

47. Ono, K.; Condron, M. M.; Teplow, D. B. Effects of the English (H6R) and Tottori (D7N) familial Alzheimer disease mutations on amyloidβ-protein assembly and toxicity. *J. Biol. Chem.* **2010**, *285*, 23186–23197.

48. a) Berhanu, W. M.; Hansmann, U. H. E. Structure and dynamics of amyloid-β polymorphism. *PLoS One* **2012**, *7*, e41479; b) C. Yang, C.; Zhu, X.; Li, J.; Shi, R. Exploration of the mechanism for LPFFD inhibiting the formation of Aβ (1-42) in water. *J. Mol. Model* **2010**, *16*, 813-821; c) Tarus, B.; Straub, J. E.; Thirumalai, D. Dynamics of Asp23-Lys28 salt bridge formation in $A\beta_{10-35}$ monomers. *J. Am. Chem. Soc*. **2006**, *128*, 16159–16168.

49. Truong, P. M.; Viet, M. H.; Nguyen, P. H.; Hu, C. K.; Li, M. S. Effect of Taiwan mutation (D7H) on structure of amyloid-β peptides: replica exchange molecular dynamics study. *J. Phys. Chem. B* **2014**, *118*, 8972–8981.

50. Wise-Scira, O.; Xu, L.; Perry, G.; Coskuner, O. Structures and free energy landscapes of aqueous zinc (II)-bound amyloid-β (1–40) and zinc (II)-bound amyloid-β (1–42) with dynamics. *J. Biol. Inorg. Chem.* **2012**, *17*, 927-938.

51. Coskuner, O.; Wise-Scira, O. Arginine and disordered amyloid-β peptide structures: molecular level insights into the toxicity in Alzheimer's disease. *ACS Chem. Neurosci.* **2013**, *4*, 1549-1558.

52. Kollman, P. A.; Massova, I.; Reyes, C.; Kuhn, B.; Huo, S.; Chong, L.; Cheatham, T. E. Calculating structures and free energies of complex molecules: Combining molecular mechanics and continuum models. *Acc. Chem. Res.* **2013**, *33(12)*, 889–897.

53. Chen, H.; Zhang, Y.; Li, L.; Han, J. G. Probing ligand-binding modes and binding mechanisms of benzoxazole-based amide inhibitors with soluble epoxide hydrolase by molecular docking and molecular dynamics simulation. *J. Phys. Chem. B* **2012**, *116(34)*, 10219-10233.

Report

ORIGINALITY REPORT

16%	0%	16%	0%
SIMILARITY INDEX	INTERNET SOURCES	PUBLICATIONS	STUDENT PAPERS

PRIMARY SOURCES

1	Rajneet Kaur Saini, Suniba Shuaib, Deepti Goyal, Bhupesh Goyal. " Insights into the inhibitory mechanism of a resveratrol and clioquinol hybrid against Aβ aggregation and protofibril destabilization: A molecular dynamics simulation study ", Journal of Biomolecular Structure and Dynamics, 2018 Publication	5%
2	Simranjeet Singh Narang, Deepti Goyal, Bhupesh Goyal. " Inhibition of Alzheimer's amyloid-β peptide aggregation by a bi-functional bis-tryptoline triazole: key insights from molecular dynamics simulations ", Journal of Biomolecular Structure and Dynamics, 2019 Publication	5%
3	Suniba Shuaib, Rajneet Kaur Saini, Deepti Goyal, Bhupesh Goyal. " Insights into the Inhibitory Mechanism of Dicyanovinyl-Substituted J147 Derivative against Aβ Aggregation and Protofibril Destabilization: A Molecular Dynamics Simulation Study ",	2%

ChemistrySelect, 2017
Publication

---

4 Krishnangsu Pradhan, Gaurav Das, Varsha Gupta, Prasenjit Mondal, Surajit Barman, Juhee Khan, Surajit Ghosh. "Discovery of Neuroregenerative Peptoid from Amphibian Neuropeptide That Inhibits Amyloid-β Toxicity and Crosses Blood–Brain Barrier", ACS Chemical Neuroscience, 2018 1%
Publication

---

5 Suniba Shuaib, Rajneet Kaur Saini, Deepti Goyal, Bhupesh Goyal. " Impact of K16A and K28A mutation on the structure and dynamics of amyloid-β peptide in Alzheimer's disease: key insights from molecular dynamics simulations ", Journal of Biomolecular Structure and Dynamics, 2019 1%
Publication

---

6 Sherri Young. "A Systematic Review of Antiamyloidogenic and Metal-Chelating Peptoids: Two Structural Motifs for the Treatment of Alzheimer's Disease", Molecules, 2018 1%
Publication

---

7 Suniba Shuaib, Bhupesh Goyal. " Scrutiny of the mechanism of small molecule inhibitor preventing conformational transition of amyloid- 1%

β monomer: insights from molecular dynamics simulations ", Journal of Biomolecular Structure and Dynamics, 2017
Publication

8	"Abeta Peptide and Alzheimer's Disease", Springer Nature, 2007 Publication	1%
9	Banafsheh Mehrazma, Arvi Rauk. "Exploring Amyloid-β Dimer Structure Using Molecular Dynamics Simulations", The Journal of Physical Chemistry A, 2019 Publication	1%

Exclude quotes	Off	Exclude matches	< 1%
Exclude bibliography	On		